SENSORLESS FAULT DIAGNOSIS OF CENTRIFUGAL PUMPS

A Dissertation

by

PARASURAM PADMANABHAN HARIHARA

Submitted to the Office of Graduate Studies of
Texas A&M University
in partial fulfillment of the requirements for the degree of

DOCTOR OF PHILOSOPHY

May 2007

Major Subject: Mechanical Engineering

SENSORLESS FAULT DIAGNOSIS OF CENTRIFUGAL PUMPS

A Dissertation

by

PARASURAM PADMANABHAN HARIHARA

Submitted to the Office of Graduate Studies of
Texas A&M University
in partial fulfillment of the requirements for the degree of

DOCTOR OF PHILOSOPHY

Approved by:

Chair of Committee,	Alexander G. Parlos
Committee Members,	Reza Langari
	Won-jong Kim
	Edgar Sanchez-Sinencio
Head of Department,	Dennis O'Neal

May 2007

Major Subject: Mechanical Engineering

ABSTRACT

Sensorless Fault Diagnosis of Centrifugal Pumps. (May 2007)

Parasuram Padmanabhan Harihara, B.E., Osmania University;

M.S., Texas A&M University

Chair of Advisory Committee: Dr. Alexander G. Parlos

Analysis of electrical signatures has been in use for some time to assess the condition of induction motors. In most applications, induction motors are used to drive dynamic loads, such as pumps, fans, and blowers, by means of belts, couplers and gear-boxes. Failure of either the electric motors or the driven loads is associated with operational disruptions. The large costs associated with the resulting idle equipment and personnel can often be avoided if the degradation is detected in its early stages, prior to reaching catastrophic failure conditions. Hence the need arises for cost-effective schemes to assess not only the condition of the motor but also of the driven load.

This work presents an experimentally demonstrated sensorless approach for model-based detection of three different classes of faults that frequently occur in centrifugal pumps. A fault isolation scheme is also developed to distinguish between motor related and pump related faults. The proposed approach is sensorless, in the sense that no mechanical sensors are required on either the pump or the motor driving the pump. Rather, fault detection and isolation is carried out using only the line voltages and phase currents of the electric motor driving the pump, as measured through standard potential transformers (PT's) and current transformers (CT's) found in industrial switchgear.

The developed fault detection and isolation scheme is insensitive to electric power supply variations. Furthermore, it does not require a priori knowledge of a motor or

pump model or any detailed motor or pump design parameters; a model of the system is adaptively estimated on-line. The developed algorithms have been tested on three types of staged pump faults using data collected from a centrifugal pump connected to a $3-\phi$, 3 hp induction motor. Results from these experiments indicate that the proposed model-based detection scheme effectively detects all staged faults with fault detection times comparable to those obtained from vibration analysis. In addition to the staged fault experiments, extended healthy operation reveals no false alarms by the proposed detection algorithm. The proposed fault isolation method successfully classifies faults in the motor and the pump without any mis-classification.

To My Parents

ACKNOWLEDGMENTS

I would like to first and foremost thank my advisor, Dr. Alexander G. Parlos, for his patient guidance and advice throughout the duration of this work. I will always cherish the numerous insightful discussions we had during the course of my stay at Texas A&M University. I would also like to take this opportunity to thank my committee members, Dr. Won-jong Kim, Dr. Reza Langari and Dr. Edgar Sanchez-Sinencio for their helpful and invaluable comments. I would like to extend my gratitude and thanks to my friends Lin Wang, Aninda Bhattacharya and Dan Ye in the Networked Intelligent Machines Laboratory for all their help and fun we shared which made my stay in College Station a pleasant one. I also wish to thank my parents, Dr. N.P.H Padmanabhan and Mrs. Brinda Lakshmy, and my brother, Ramesh, for their love and unending source of inspiration. Finally, I would like to thank my beloved wife, Bharati, from the bottom of my heart for her unconditional love and support.

TABLE OF CONTENTS

CHAPTER Page

Page

LIST OF TABLES

LIST OF FIGURES

FIGURE Page

FIGURE Page

FIGURE Page

CHAPTER I

INTRODUCTION

A. Motivation

Motor current signature analysis (MCSA) and electrical signal analysis (ESA) have been in use for some time to estimate the condition of induction motors based on spectral analysis of the motor current and voltage waveforms. In almost all applications, motors are always coupled to other dynamic systems. Consequently, it would be more beneficial if the drivepower system as a whole is monitored. A drivepower system includes the electronic drive and control packages, motors, shafts, couplers, belts, chains, gear drives, bearings, pumps, conveyors, etc. As time passes, all of the individual system components of the drivetrain degrade and finally some component catastrophically fails resulting in an unscheduled shutdown. The large costs associated with the resulting idle equipment and personnel can often be avoided if the degradation is detected in its early stages [1]. Hence there is a need for an effective diagnosis scheme not only for condition assessment of the motor, but also for the rest of the drivetrain. This work deals with the sensorless diagnosis of faults that occur in centrifugal pumps driven by induction motors.

A point to note is that the proposed approach is "sensorless" in the sense that no mechanical or process-based sensors are used for the detection and isolation of faults that occur within centrifugal pumps. Only the motor electrical signals are used. The motor line voltages and phase currents can be measured using potential transformers (PT's) and current transformers (CT's), which are standard installations in most of the industries and are easily accessible.

The journal model is *IEEE Transactions on Automatic Control.*

A lot of effort has been invested in detecting and diagnosing incipient faults in centrifugal pumps through the analysis of vibration data, obtained using accelerometers installed in various locations on the pump. Fault detection schemes based on the analysis of process data, such as pressure, flow and temperature have also been developed. In some cases, speed is used as an indicator for the degradation of the pump performance. All of the above mentioned schemes require sensors to be installed on the system. Installation of these sensors leads to an increase in overall system cost. Additional sensors need cabling, which also contributes towards increasing the cost of the system. These sensors have lower reliability, and hence fail more often than the system being monitored, thereby reducing the overall robustness of the system. In some cases it maybe difficult to access the pump to install sensors. One such example is the case of submersible pumps wherein it is difficult to install or maintain sensors once the pump is underwater. To avoid the above-mentioned problems, the use of mechanical sensors has to be avoided to the extent possible. Since many of the industrial pumps currently in use are centrifugal pumps (about 90% [2]) and most are driven by induction motors, the present work concentrates on analyzing the motor line currents and line voltages to detect and diagnose faults occurring in centrifugal pumps.

A fault diagnosis scheme consists of three stages, which are described below:

1. *Stage 1 - Fault Detection:* This stage involves analyzing the fault features extracted from the sampled signals and detecting the presence of a fault in the system. The output of this stage informs the plant supervisor or the manager that the system under supervision is not performing up to its standards. There is no further information as to which component within the system is faulty and what type of fault is present.

2. *Stage 2 - Fault Isolation:* Once it has been established that there is a fault in the system the next stage is to locate the fault and determine the faulty component. This would save time for the maintenance personnel in deciding the course of action to be taken to get the system back online. Moreover, the equipment/production downtime would be reduced drastically as the personnel would not be dismantling many components to establish the cause of the downtime.

3. *Stage 3 - Fault Identification:* Once the faulty component is determined, the downtime can be further reduced if the maintenance personnel have information about the type of fault. For example whether the fault is of mechanical or electrical origin. This would enable them to be ready with the necessary spare parts or the repair personnel to replace or repair the faulty part of the component.

This work deals only with the first two stages of the fault diagnosis scheme.

B. Problem Definition

The objective of this work is to develop and validate an efficient, sensorless fault detection and isolation scheme for operational and mechanical faults that occur within centrifugal pumps. The developed scheme must not generate false alarms arising due to changes in the power supply or load and/or load pulsations. At the same time, the scheme must have a high probability of fault detection and enable the distinction between motor and pump faults.

C. Literature Survey

Most of the literature on fault detection of centrifugal pumps is based on techniques that require the measurement of either vibration or other process based signals. There are very few references that deal with sensorless or non-invasive/non-intrusive techniques to diagnose faults in centrifugal pumps. Moreover, in all the literature presented, the motor is considered to be "healthy". No experiments are performed to determine whether the fault exists in the motor or in the pump. Faults are only staged in the pump and this knowledge is used in the detection of pump faults. But in reality, this information is seldom available. In [3], the authors review the latest techniques that are employed in pump diagnostics. A list of typical pump problems that develop in the pump along with the conventional method of detection is presented.

In [4], the development and application of signal processing routines for the condition monitoring of water pumps used in submarines is discussed in detail. Eroded impeller condition of a Bryon Jackson Sea Water Pump, which is a centrifugal pump, found in submarines is investigated. The eroded condition affects the mechanical load and the amount of torque provided by the three phase induction motor. It is postulated that changes in the load torque would lead to changes in the input power driving the induction motor. Hence fault features related to eroded impeller conditions are extracted from the power spectrum using the signal processing algorithms developed and these features are used as indicators for fault diagnosis. A classification scheme based on the nearest neighborhood technique is also developed. Using this technique, 90% of the test cases are classified correctly. A neural network-based scheme is also developed to improve the classification accuracy.

In [5, 6, 7, 8], the authors point out that the operation of the pump away from its best efficiency point (BEP) has been a significant source of pump problems. Unsteady

hydraulic forces are the dominant sources of overall loads for centrifugal pumps. In this work, motor current and power analysis has been shown to be an alternative for the detection of some of the operational and structural problems related to pumps. Some of the cases considered are:

- Load stability versus flow rate,
- Equipment misalignment and
- Clogged suction strainer.

A comparative study between the vibration spectrum, power spectrum and the torque ripple spectrum is undertaken in the detection of the above-mentioned case studies. In these studies, the underlying assumption is that the motor speed, current, power and power factor change in response to load changes or fluctuations. The idea is to monitor the load related peaks in the power or current spectrum. Since the motor power changes relatively linearly with load as opposed to the nonlinear relationship between the current and the load, the motor power is considered as the parameter to be monitored. The running speed harmonic is one of the indicators monitored in the power spectrum to establish the condition of the pumps under consideration. It is concluded that although vibration spectra obviously provided critical equipment health information, the motor current and the power spectra analysis offered an attractive alternative in diagnosing the condition of the pumps.

Some of the submersible pumps in operation today are at a depth of more than 1000 meters. Therefore the use of vibration sensors for pump and motor protection and condition monitoring is difficult due to the extreme conditions and remote locations. Motor current signature analysis (MCSA) offers an attractive alternative for the condition monitoring of these pumps. For example, if a pump is running under

improper conditions, the torque transmitted from the motor to the pump will be influenced. Non-stationary torque changes cause non-stationary changes in the rotor speed inducing amplitude modulation of the motor current. In [9], motor currents are analyzed to detect some of the faults that occur in centrifugal pumps, namely, partial flow operation, reverse rotation, disturbed inflow condition, cavitation, air suction and bearing failures. The energy content of the current signal in the frequency range of 2 Hz to 10 Hz is considered as an indicator. Depending on the changes in the noise floor level in certain operating regions of the pump, the above-mentioned faults are diagnosed.

The work in [10] deals with the development of a multi-model fault diagnosis system of an industrial pumping system. The system under consideration is a seawater pumping system in operation at the Nuclear Electric "Heysham 2" power station. The system is based around the operation of two centrifugal pumps with associated valves, motors and pipework. This system can have two different type of faults; incipient, slowly-developing faults whose effects may be difficult to distinguish from normal operating condition changes and abrupt severe faults which must be detected immediately. A detailed nonlinear and linear simulation model of the two-pump system is developed, of which the linear model is used as the basis for fault detection and isolation. Two different approaches to model-based fault detection are outlined based on observers and parameter estimation. For the observer based methods, the motor current, the suction and the discharge pressures are monitored. A vector of residuals was formed from the outputs of the observer and the actual outputs (in these cases, simulations). The deviation of these residuals from zero indicates the presence of a fault. Similarly a simplified model was developed for parameter estimation case. The relationship between the model coefficients and the physical parameters of the system was developed. Residual signals were formed by comparing

each on-line calculated parameter with the respective known parameter values derived from known fault free situations. The results showed that the majority of these faults were identified by their effect on the different residuals. The authors also point out that the observer method and the parameter estimation method can be combined for more effective fault diagnosis.

In [11], the motor current is used as a diagnosing signal to estimate the following faulty conditions in pumps:

- cavitation (including low-level cavitation as a separate fault),
- blockage (including low-level blockage as a separate fault) and
- damaged impeller.

Fault signatures are established by relating the spectral features to individual faults and by analyzing their behaviour in the presence of faults. Eight attributes are chosen to characterize the three faults considered. A fuzzy logic system is then designed to classify the faults. The consistency of the selected attributes is established so that they could be used as inputs to the fuzzy logic system, which performs the evaluation based on the rules set and finally makes a decision on the pump condition. The fuzzy logic system is developed using data collected from a centrifugal pump and is tested and evaluated with data collected from another centrifugal pump. The probability of fault detection varies from 50% to 93%. The authors finally conclude that adjustments to the rules or the membership functions are required so that differences in the pump design and operating flow regimes can be taken into consideration. They also point out that, in industrial setups the pump type, size and performance specifications are fixed and are unlikely to undergo any change.

In [12, 13], electrical signature analysis (ESA) is extended to condition monitoring of aircraft fuel pumps. While considerable amount of data are acquired from both

main and auxiliary pumps, the data analysis is concentrated on data obtained from the auxiliary pumps. Among the various degraded conditions observed, the bearing wear is selected to demonstrate the effectiveness of ESA in determining the pump condition. Moreover, inspection of the auxiliary pumps shows that the front bearing wear is more common than the rear bearing wear, since the front bearing/journal clearance is mostly greater than the rear bearing/journal clearance in almost all the cases considered. After considerable study, it is established that the best indicator of front bearing wear in the motor current spectrum is not any specific frequency peak but is the base or floor of the spectrum. The noise floor of the demodulated current spectrum at dead-head (zero flow) conditions is observed to increase in all the pumps having degraded front bearings. The authors also point out that methods for detecting other pump degradations would be developed.

In [14], a model-based approach using a combination of structural analysis, observer design and analytical redundancy relation (ARR) design is used to detect faults in centrifugal pumps driven by induction motors. Structural considerations are used to divide the system into two cascaded connected subsystems. The variables connecting the two subsystems are estimated using an adaptive observer derived from the equations describing the first subsystem. The fault detection algorithm is based on an ARR which is obtained using Groebner basis algorithm. Four different types of faults, namely, clogging inside the pump, dry running, rub impact and cavitation are staged to test the validity of the algorithm. The measurements used in the development of the fault detection method are the motor terminal voltages and currents and the pressure delivered by the pump.

In [15], a fault detection scheme has been discussed, which assumes that the torque and the speed of the motor can be measured and that either the differential pressure between the suction and discharge, or the pump flow can be measured. The

measured process variable is compared to that which is computed based on the motor speed and torque. An important point to note is that, an inherent assumption is made regarding the health of the motor. It is assumed that the motor is healthy. The measured parameters also change if the motor develops a fault or if the load level is changed.

In [16], a diagnosis scheme to detect the low flow and/or cavitation condition in centrifugal pumps using the current and the voltage data of the motor is patented. These signals are conditioned, which includes amplification, anti-aliasing, etc. They are sampled at a rate of approximately 5 kHz. From the sampled voltage and the current signals, a power signal is determined by multiplying the voltage and the current values. The power signal is then re-sampled to 213.33 Hz. This signal is then used to compute a 1024 point FFT, with a frequency resolution of around 0.208 Hz. The spectral energy within the band of about 5 to 25 Hz is calculated and the noise energy in this region is compared to the baseline signal. If the difference exceeds a certain fixed threshold value, a warning signal is raised. The authors also propose an alternate method for detecting the low flow/cavitation using a digital band-pass filter as opposed to an FFT to generate the output that represents the energy content around the 5 to 25 Hz range. In this case though, the signal is re-sampled to 500 Hz and the region of interest is reduced to 5 to 15 Hz as the filter must attenuate frequencies over 25 Hz without a complex transfer function. In [17], the authors describe a fault detection system for diagnosing potential pump system failures using fault features extracted from the motor current and the predetermined pump design parameters.

Most of the literature presented above deal with detecting pump faults either by using vibration and process measurements or by using physics based models. The drawbacks of using vibration and process sensors were outlined earlier and the need to

avoid mechanical sensors was established. The models developed depend on the pump design parameters, which are not easily available and hence the detection schemes presented in the literature are not easily portable to other pump systems. Some of the studies however, use motor electrical signals to detect pump faults, but these detection schemes are based on either tracking the variation of the characteristic fault frequency or computing the change in the energy content of the motor current in certain specific frequency bands. The fault frequency depends on the design parameters, which are again not easily available. For example, the rolling element bearing fault frequency depends on the bearing diameter, pitch, number of rollers, etc. This information is not available, unless the pump is dismantled. Changes in the energy content of certain frequency bands could also result due to changes in the power supply or changes in the load even without any fault in the pump. Hence, this would result in the generation of frequent false alarms. Moreover, none of the literature mentioned above deal with the distinction between motor and pump faults.

D. Research Objectives

Based on the previous section, it can be seen that there is not only a strong need to develop a non-intrusive/non-invasive and sensorless fault detection algorithm to detect faults in centrifugal pumps but also the developed scheme must be insensitive to false alarms and must be independent of the motor and pump design parameters. Moreover, a fault isolation scheme has to be developed to distinguish between motor faults and pump faults. The research objectives can be summarized as follows:

- Develop a sensorless fault detection and isolation method to
  - detect faults in centrifugal pump.
  - distinguish between motor faults and pump faults.

- The desired performance characteristics are:
  - exhibit high probability of fault detection.
  - exhibit low probability of false alarms.
  - continuous monitoring system.
  - independent of motor and pump design information.

E. Proposed Approach

The objectives of the proposed research can be achieved by dividing them into three phases, which are as explained below:

1. Phase 1: The first task consists of controlled experiments of the various anticipated healthy conditions of the centrifugal pump. The pump curves at the healthy state of the pump will be established through these experiments and the best efficiency region of the pump will be determined. Performance metrics pertaining to the cavitation conditions will be established in order to approximately quantify the effects of operational faults in centrifugal pumps.

2. Phase 2: In this phase, the motor line currents and line voltages will be sampled and analyzed to extract fault features pertaining to the operational and structural problems of the pump. The first step would be to carry out signal segmentation of the motor currents and analyze only the stationary parts of the signal. Digital signal processing techniques such as FFT analysis will be used to extract the different fault features. The second step will be to develop a generalized early fault detection scheme based on the extracted fault features. This will be based on recent work in [18, 19] that describes the development of a sensorless system for the detection of both mechanical and electrical incipient

faults developing in induction motors. The detection effectiveness of the system has been experimentally demonstrated on motors of varying power rating [18]. Furthermore, the false alarm reduction effectiveness of the system has also been experimentally demonstrated [19].

3. Phase 3: This is the final phase, which deals with the design of a fault isolation algorithm to distinguish between faults occurring in the pump and the motor. Higher order spectra will be used to distinguish between motor and pump faults.

F. Research Contributions

This work concentrates on developing and validating a sensorless fault diagnosis algorithm for centrifugal pumps that is based on the analysis of the motor currents and voltages only and it is independent of a priori motor and pump model and/or parameters. The contributions of this work can be summarized as follows:

- Use of the motor currents and voltages to detect some of the most commonly encountered faults in centrifugal pumps.
- Design and evaluation of a fault isolation scheme, to differentiate between faults in centrifugal pumps and motors that are used to drive them.
- The fault detection and isolation algorithms are:
  - insensitive to motor electric power supply variations.
  - insensitive to pump load changes or load fluctuations.
  - independent of a priori motor and pump models and/or design parameters.

Thus the proposed fault diagnosis approach is considered quite portable to motor-pump systems of different size and manufacturer.

G. Organization of Dissertation

In Chapter II, a brief overview of centrifugal pumps and principles of operation are discussed. Some of the common failure modes of centrifugal pumps are also presented.

In Chapter III, an overview of signal-based and model-based fault detection methods are described. The basic principle involved in detecting pump faults using motor electrical signals is also discussed in detail.

In Chapter IV, the details of the proposed model-based fault detection and isolation methods are presented. The development of the fault detection and isolation indicators are described in some detail.

In Chapter V, the experimental results obtained in this research are presented in detail. A brief discussion of the experimental setup used for the validation of the proposed fault detection and isolation methods is also discussed.

In Chapter VI, a summary of the work, conclusions drawn from this research and directions for future research are presented.

CHAPTER II

PUMP OPERATION AND FAILURE MODES

A. Pump Classification

Pumps are mainly used to transfer liquids from low pressure zones to high pressure zones. They are classified based on the principle by which energy is added to the fluid being pumped. The two principal families are kinetic energy pumps and positive displacement pumps. A pump classification tree is shown in Figure 1. Positive displacement pumps perform work by expanding and then compressing space within the pump. They actually capture the liquid and physically transport it through the pump to the discharge nozzle. Reciprocating pump is an example of such a type of pump. Kinetic energy pumps can be further subdivided into centrifugal pumps (the vast majority of pumps) and special effects pumps. Jet pumps, reversible centrifugal, gas lift and electromagnetic pumps are some examples of special effect pumps. Centrifugal pumps generate pressure by accelerating and then decelerating the movement of the liquid through the pump. These pumps can be further classified based on the position of the pump shaft (horizontal or vertical), the way in which liquid enters the eye of the impeller (single-suction or double suction), type of flow (axial or radial or mixed), number of impellers (single-stage or multi-stage), etc. The impellers used in these pumps are also classified as closed, semi-open and open. A closed impeller has side walls that extend from the eye to the outer edge of the vane tips; an open impeller does not have side walls, whereas a semi-open impeller has side walls extending only on one side. Since about 90% of the pumps used in industry are centrifugal pumps [2], the present research concentrates on diagnosing faults arising in centrifugal pumps. Specifically, the centrifugal pump under consideration is a single-stage, single suction,

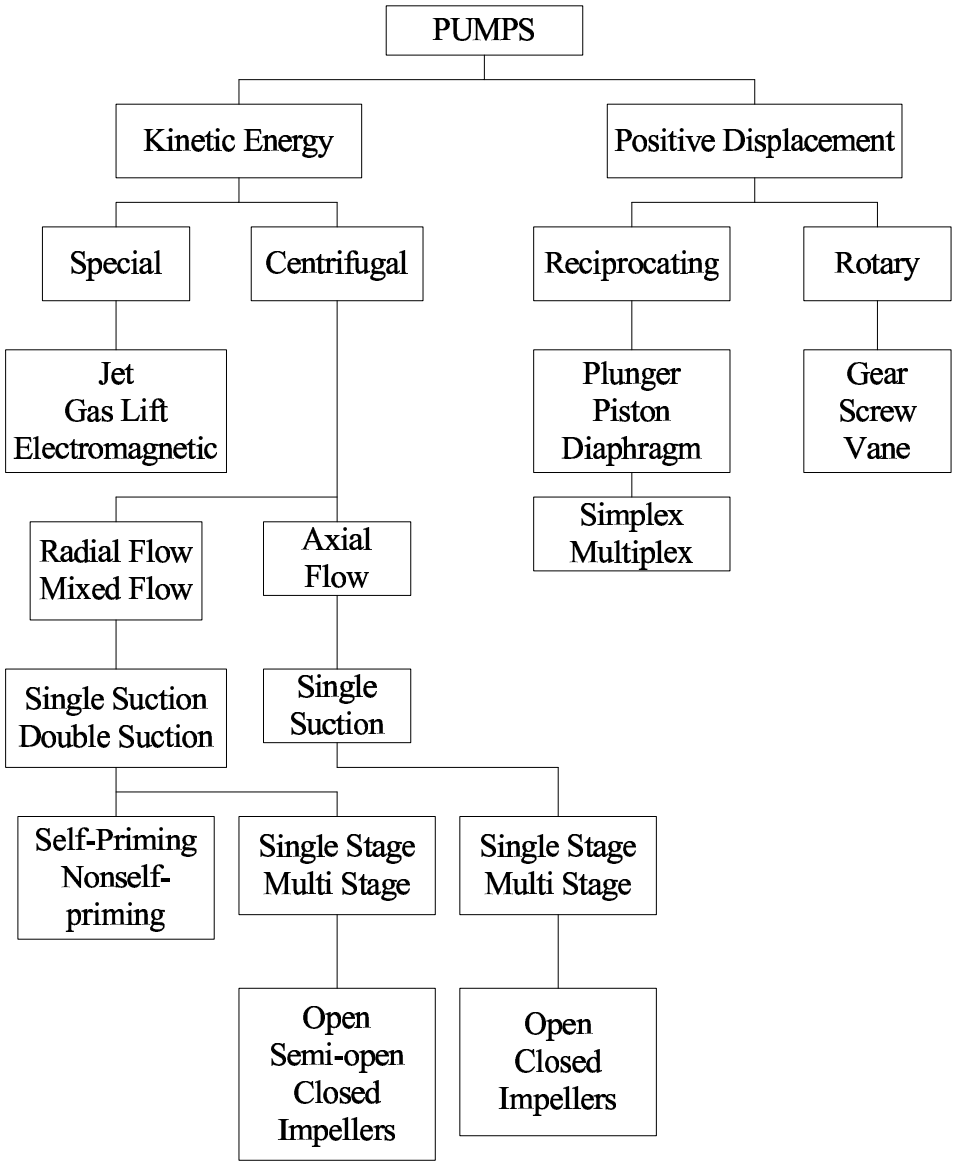

Fig. 1. Pump classification tree [20].

nonself-priming, open impeller, radial flow pump.

B. Centrifugal Pumps - Basics and Principles of Operation

The principle pumping unit of a centrifugal pump is the volute and the impeller, as shown in Figure 2. The liquid enters into the eye of the impeller and is trapped between the impeller blades. The blades impart speed to the liquid as it moves towards the tip of the blade. As the liquid accelerates in velocity, a zone of low pressure is created in the eye of the impeller (the Bernoulli principle, as the velocity goes up, pressure goes down). The liquid leaves the outer diameter of the impeller at high speed and immediately slams into the internal casing of the volute. At this point, the liquids centrifugal velocity is equal to zero and the velocity is converted to pressure. Since the motor is spinning, the liquid still has rotary velocity. The liquid is then conducted around the internal volute housing in an ever increasing escape channel. As the pathway increases, the rotary velocity decreases and more pressure is added to the liquid, which leaves through the discharge nozzle prepared to overcome the resistance in the system [2, 21].

The operation of pumps is governed by laws known as “affinity laws”. These are a group of rules that can be used to determine the operational characteristics of the pump when the pump velocity changes. These rules are shown below:

$$\begin{aligned} Q &\propto N \\ H &\propto N^2 \\ BHP &\propto N^3 \end{aligned} \tag{2.1}$$

where ’Q’ is the liquid volume measured in gallons per minute (gpm), ’H’ is the total head measured in feet, ’N’ is the shaft velocity measured in revolutions per minute

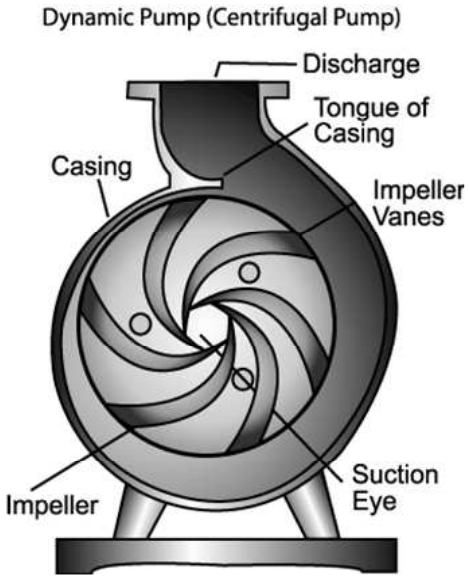

Fig. 2. Inside of a centrifugal pump [22].

(rpm) and 'BHP' is the brake horsepower measured in horse power (hp).

The performance of a pump is characterized by means of the interrelations between the pump head, efficiency, flow and the brake horsepower. These interrelations can be graphed on a chart and this chart is commonly referred to as the *pump-characteristic curves*. The pump-characteristic curve is actually four curves on a common graph:

1. The Head-Flow Curve; it is called the H-Q curve,
2. The Efficiency Curve,
3. The Energy Curve, and
4. The Pump's Minimum Requirement Curve; this is called Net Positive Suction Head Required, NPSHr.

A typical centrifugal pump performance chart is shown in Figure 3. As flow increases, the total head starts to drop gradually. The brake horsepower (BHP) generally increases linearly with flow. The efficiency curve is in the form of a bell curve, with the peak point termed as the best efficiency point (BEP). The net positive suction head required (NPSHr) remains flat till the BEP zone. Once the curve crosses the BEP value, the NPSHr increases exponentially. It is advisable to operate a pump at or near the BEP zone. Operation of a pump to the far left or far right of the BEP zone is detrimental and the consequences of such an operation are discussed in some detail in later sections.

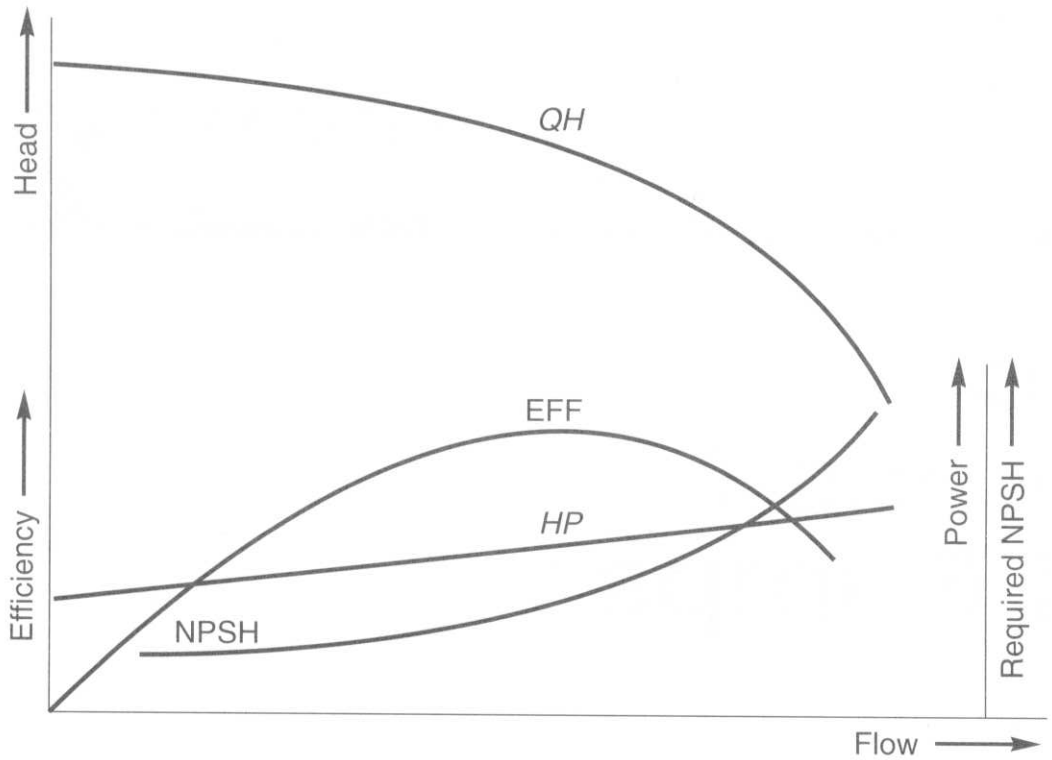

Fig. 3. Typical performance curves of a centrifugal pump [23].

C. Common Failure Modes in Centrifugal Pumps

Pump failures can occur either due to improper operational conditions or mechanical damage. Some of the most common adverse consequences arising due to poor maintenance and improper operation of pumps are described in the following subsections in no particular order.

1. Cavitation

Cavitation is defined as the formation and subsequent collapse or implosion of vapor bubbles in the pump. It occurs because the absolute pressure on the liquid falls below the liquids vapor pressure. If cavitation occurs in a pump, then its efficiency is reduced. It can also cause sudden surges in flow and pressure at the discharge nozzle. The effects of cavitation are noise and vibration. There are five recognized types of cavitation [2]. Each type of cavitation is briefly explained below:

- *Vaporization cavitation:* This is also known as the "classic cavitation" and it is mainly caused from the inadequate net positive suction head available (NPSHa). This type of cavitation accounts for around 70% of all pump cavitation problems. The damage from vaporization cavitation can be seen behind the impeller blades towards the eye of the impeller.

- *Internal recirculation cavitation:* This is a low flow condition where the discharge flow of the pump is restricted and the liquid is forced to re-circulate from high pressure zones in the pump into the low pressure zones across the impeller. This type of cavitation originates from two sources. First, the liquid is circulating inside the volute of the pump at the speed of the motor and it rapidly overheats. Second, the liquid is forced to pass through tight tolerances at very high speed. The heat and the high velocity cause the liquid to vapor-

ize. With open impellers, the damage can be seen on the leading edge of the impeller blades towards the eye of the impeller and on the blade tips towards the impellers outer diameter (OD). On enclosed impellers, the damage reveals itself on the wear bands between the impeller and the volute casing.

- *Vane passing syndrome:* This can exist when the blade tips at the OD of the impeller are passing too close to the cutwater on the pump casing. The free space between the impeller blade tips and the cutwater should be around 4% of the impeller diameter.

- *Air aspiration:* If a mixture of air and liquid enters the impeller, then the centrifugal forces generated by the rotating blades throw the heavier liquid outward, thus trapping the air in the center of the pump. Under certain conditions, enough air is trapped in the eye of the impeller, that it separates the liquid in the suction line completely from the liquid at the outer radii of the impeller. Depending on the amount of air trapped in the eye of the impeller, this displaced air can fully or partially block the inlet to the impeller vanes. In the first case, the pump is not able to deliver any liquid. In the second case, the pump may start to deliver reduced amount of liquid provided that it can develop sufficient head to overcome the resistance of the system. There are two sources of air entering a centrifugal pump: air pockets and air leakage. Air pockets can occur in the suction line, the pump casing or the discharge line. Air leaks into the piping and pump in diverse forms and at different points [23]. This type of cavitation manifests itself similar to the vaporization cavitation, but the solution is different. To prevent this type of cavitation, all the points of entrance and escape has to be sealed effectively.

- *Turbulence cavitation:* This results from the turbulence caused by formation of

vortexes in the suction flow and/or inadequate piping, sharp elbows, restrictions, etc.

If a pump operates under cavitation conditions for sufficient amount of time, the following can occur:

- Pitting marks on the impeller blades and on the internal volute casing wall of the pump,
- Premature bearing failure,
- Shaft breakage and fatigue failures in the pump, and
- Premature mechanical seal failure.

These problems arise from one or more of the following:

- A reduction in the pressure at the suction nozzle,
- An increase in the temperature of the pumped liquid,
- An increase in the velocity or flow of the fluid,
- Undesirable flow conditions caused by sharp elbows in the suction piping, and
- The pump is inadequately sized for the system.

2. Very Low or Zero Flow Operation

This condition occurs when a pump does not deliver the required flow rate or does not pump sufficient amount of liquid even at the maximum speed. This arises when a pump is operating far to the left of the BEP zone. This results from severely over-designing the pump for the system. Under partial load conditions, excessive

recirculation of the liquid can be observed. This causes the liquid to overheat. The liquid enters the impeller at an angle smaller than the blade angle. This creates a dead space in the region, where cavitation usually begins to develop. The pump suffers from high head and pressure, radial loading, shaft deflection and high vibrations that can affect the motor and the pump bearings. All these conditions lead to loss of pumping efficiency. The problems caused by recirculation increase with increasing pump size and speed.

3. Dry Running

Dry running occurs when a pump is operating under insufficient or no liquid in the pump. The nonself-priming centrifugal pumps can only operate if the volute of the pump is completely filled with liquid. If the volute is not completely filled with the fluid to be pumped then dry running occurs thereby causing significant damage to the internal components of the pump, resulting in decrease of pumping efficiency. If this condition is prolonged, then the pump eventually breaks down altogether [24].

Apart from the operational problems discussed above, some of the other commonly encountered problems include reverse rotation, which results in a low flow of approximately 60% of the design flow during startup [25] and disturbed inflow and outflow conditions, wherein the suction and the discharge are clogged. In addition to these failures, some of the mechanical problems encountered in the case of centrifugal pumps are discussed briefly in the following subsections.

4. Bearing Failures

The pump bearings used are either sleeve bearings or rolling element bearings. Ball bearings have almost completely replaced the sleeve bearings in pumps designed today. Rolling element bearings have round balls or rollers, which move within the

inner ring or race and outer ring or race. The inner ring mounts onto, centers and rotates with the spinning shaft, while the outer ring is stationary and press-fit into the bore of the pump. Even though the cost of the bearings might be relatively low, the direct and indirect costs associated with the replacement of the bearings can be substantial. Most likely, the failure is the result of abnormal operating conditions or lack of proper bearing maintenance. Some of the most common causes of premature bearing failure include improper mounting of the bearing on the shaft, dirt and abrasion, which accounts for roughly 90% of bearing failures as indicated by some studies [2], inadequate lubrication, etc.

5. Damage to the Pump Impeller

The impeller is the "heart" of the pump. Any failure to the impeller results in the reduction of flow, thereby resulting in a decrease in the efficiency of the pump. There are various types of failure modes associated with the pump impeller. Some of them are itemized below:

- The impeller is mounted loosely onto the shaft,
- The geometry of the impeller gets altered due to internal wear and tear, and
- Cracks develop in the impeller vanes.

6. Degradation of Mechanical Seals

Mechanical seals are preferred over conventional packing seals, form a barrier between the rotary and stationary parts in the pump. The seal must block leakage at the following three interface points:

- the rotary and stationary faces of the seal,

- the stationary element and the seal chamber housing of the pump, and
- the rotary element and the shaft or sleeve of the pump.

Most of the manufactured mechanical seals incorporate o-rings as secondary seals. By design, the weakest point in the centrifugal pump is the mechanical seal. Therefore, any instability in the rotating element, caused by either mechanical or process imbalance can lead to premature seal failure. About 80% of the pumps employed in the chemical industry are withdrawn because of mechanical seal failures [26]. About half of all pumps pulled out of service are either leaking or could not hold pressure or pump liquid. This is most likely an o-ring failure. Some of the most common causes of seal failure include cavitation, running the pump dry and running the pump with closed discharge for extended periods of time [25].

Some of the other commonly encountered problems include reverse rotation, which results in a low flow of approximately 60% of the design flow during startup [25]; disturbed inflow and outflow conditions, wherein the suction and the discharge are clogged; motor and pump shaft misalignment, which can lead to premature bearing and mechanical seal failures; and shaft deflection.

A recent study on pump failure modes indicate that the most common cause of pump failure is the failure of the sealing device [27]. Figure 4 shows the different types of pump failures as given in [27]. However, failure of the seals does not occur due to inherent product weakness, but due to the fact that about 91% of the time the seal is being pushed to premature failure. Figure 5 shows some of the causes for premature seal failure as mentioned in [27]. Only about 8% of the times, the seal fails due to inherent faulty component when compared to about 40% of the times due to operational conditions such as cavitation, etc and about 24% of the times due to mechanical problems like bearing damage or impeller damage.

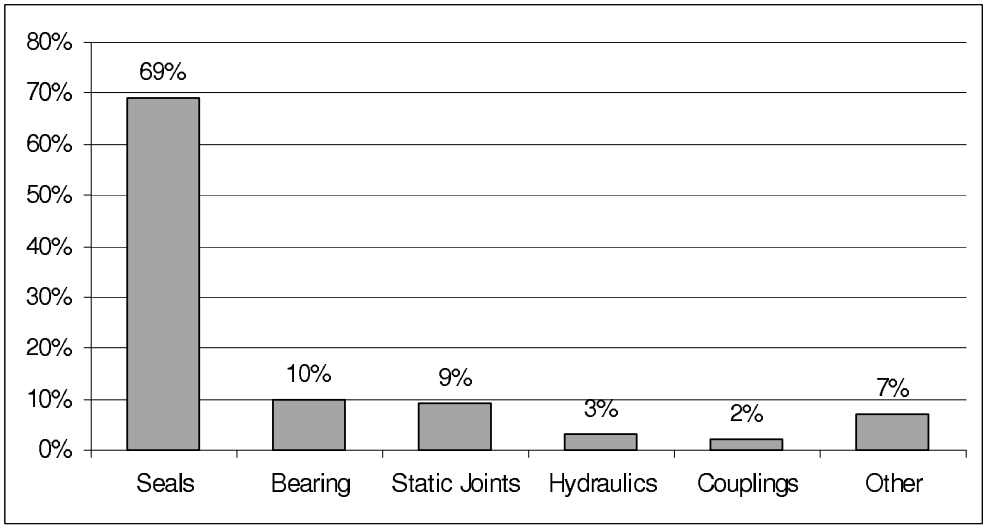

Fig. 4. Common types of pump failures.

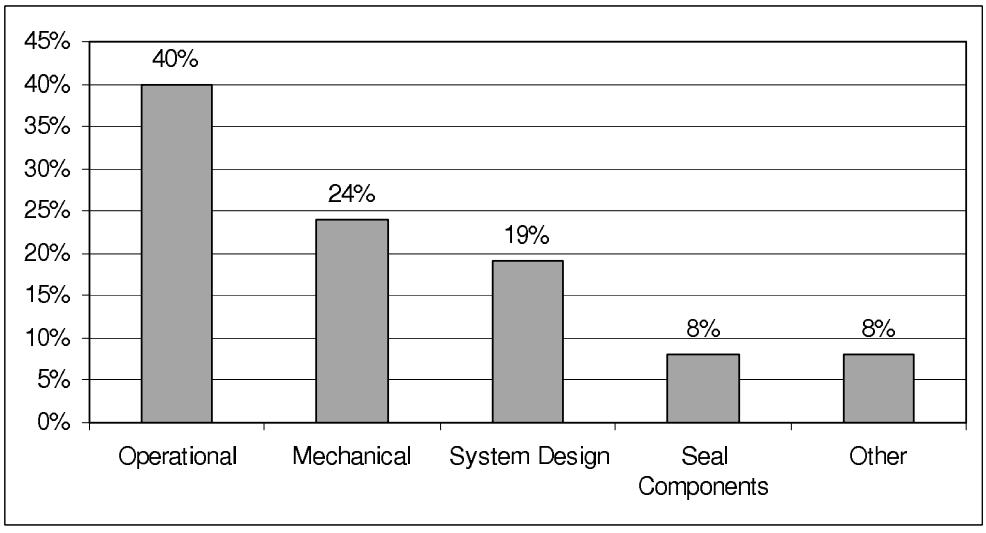

Fig. 5. Causes for premature seal failure.

CHAPTER III

OVERVIEW OF FAULT DETECTION METHODS

A. Introduction

Maintenance practices employed in various industries have varied over the past decade. These practices can be broadly classified as

- *Reactive Maintenance:* This is basically the "run till failure" approach. No maintenance action is taken until the equipment fails and once the equipment breaks down it is either repaired or replaced depending on the amount of budget allocated. Although it may seem that money is being saved on maintenance costs and labor costs, actually more money is spent in the long run on the repair costs and the purchase of new equipment. The life of the equipment is actually shortened while waiting for the equipment to break-down. This results in more frequent equipment replacements. One of the major concerns of this approach is the unplanned downtime of equipment resulting in loss of production and hence reactive maintenance results in equipment being operated inefficiently for extended periods resulting in increased energy costs.

- *Preventive Maintenance:* This refers to routine scheduled maintenance. Equipment are tested for their performance on a time-based schedule or are tested based on the machine run-time. Although this type of maintenance procedure is better than reactive maintenance, it still cannot prevent unplanned downtime of equipment and includes unnecessary maintenance activities which might result in the damage of other components.

- *Predictive or Proactive Maintenance:* This approach is based on the fact that

Table I. Maintenance procedures employed in industry [28].

Maintenance Procedure	Percentage (%)
Reactive Maintenance	55%
Preventive Maintenance	31%
Predictive Maintenance	12%
Other	2%

equipments are periodically or continuously monitored and if any anomaly is detected, maintenance is scheduled. Predictive maintenance differs from preventive maintenance because the maintenance needs are based on the actual condition of the equipment rather than some pre-determined schedule. This method can substantially reduce the unplanned downtime of equipment thereby enabling greater plant availability and smoother plant operations. In addition it can enhance energy efficiency by reducing the time equipments operate with damaged components. This approach is also referred to as Condition Based Maintenance (CBM).

Recent studies [28] indicate that the predominant form of maintenance procedures employed in industries is still reactive maintenance. Table I gives a breakdown of the maintenance programs used in various industries. The present work primarily deals with formulating a centrifugal pump fault detection and isolation method that can be used within a continuous CBM system.

The different detection scenarios available for any fault detection method are shown in Figure 6. It can be concluded that, for the fault detection method to perform effectively, it must exhibit a high probability of fault detection and a low probability

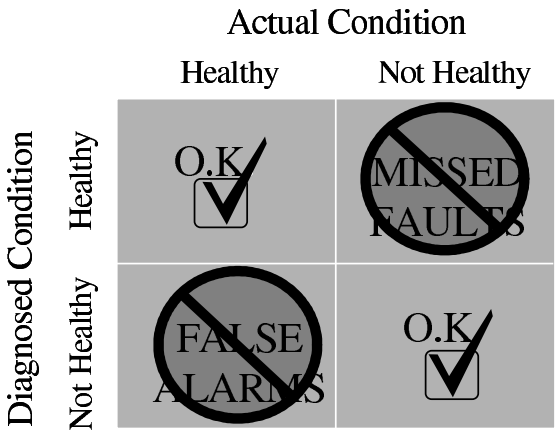

Fig. 6. Fault detection scenarios.

of false alarms. If the detection scheme is too sensitive then it is likely to generate false alarms which in turn would lead to operators questioning the effectiveness of the algorithm. At the same time if the detection scheme is too insensitive, the false alarms will be reduced but then there is a chance of missing anomalies and faults that might lead to a failure. Missed faults may lead to critical equipment failures leading to downtime. As a result, a balance must be achieved in designing a fault detection scheme that is sensitive to faults but insensitive to false alarms.

B. Classification of Fault Detection Methods

The fault detection methods can be broadly classified into two groups, namely, signal-based fault detection methods and model-based fault detection methods. A brief overview of the two methods are described in the following two subsections.

1. Signal-Based Fault Detection Methods

Signal-based fault detection techniques are based on processing and analyzing raw system output measurements, such as motor currents, vibration signals and/or other process-based signals. No explicit system model is used in these techniques. Fault features are extracted from the sampled signals and analyzed for the presence or lack of a fault. The basic schematic of a signal-based fault detection method is as shown in Figure 7.

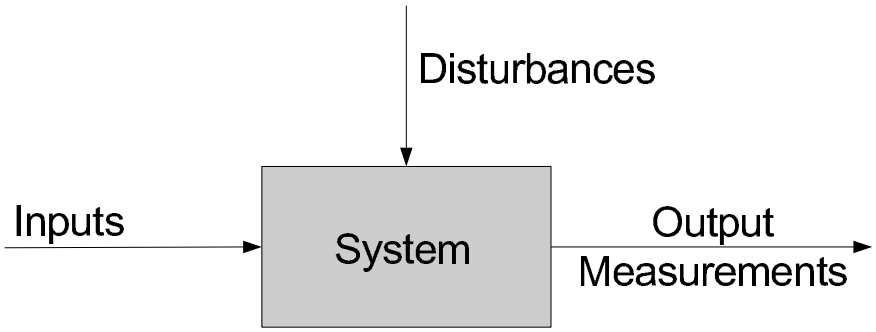

Fig. 7. Signal-based fault detection method.

The output measurements are the sampled signals that are analyzed to check for the presence or lack of a fault within the system. However, these system output signals are impacted by changes in the operating conditions that are caused due to changes in the system inputs and disturbances. Hence, if one were to analyze only the system output signals for the presence of a fault, then it would be difficult to distinguish the fault related features from the input and disturbance induced features. This would result in the generation of frequent false alarms, which would in turn result in the plant personnel losing confidence over the fault detection method. If the system inputs are considered to be ideal, i.e.,there are no changes in the input and a constant input is supplied to the system and the disturbances are also assumed to be constant, then the signal-based detection schemes can be used in the detection of system faults

with 0% false alarm rates. However, in reality such a case is not possible. The input variations cannot be controlled and harmonics are injected into the system inputs due to various reasons. Moreover, the system disturbances are also never constant. Hence these variations affect the system output signals and result in the generation of false alarms.

2. Model-Based Fault Detection Methods

The framework of a model-based fault detection method is as shown in Figure 8. The

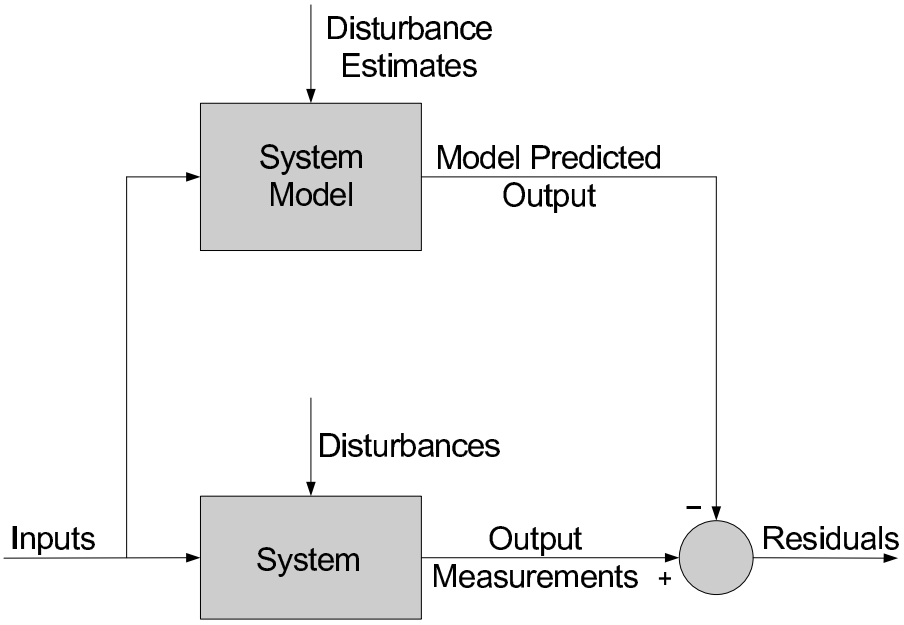

Fig. 8. Model-based fault detection framework.

basic principle of a model-based fault detection scheme is to generate residuals that are defined as the differences between the measured and predicted outputs. The system model could be a physics-based model or an empirical model of the actual system being monitored. The model defines a relationship between the system outputs and the system faults, system disturbances and system inputs. The measured variables

are the system inputs and outputs and the predicted variables are the outputs of the system model. Ideally, these residuals are only affected by the system faults and not affected by any changes in the operating conditions due to changes in the system inputs and disturbances. That is, the generated residuals are only sensitive to faults while being insensitive to system input or disturbance changes [29]. If the system is "healthy", then the residuals would be approximated by white noise. Any deviations of the residuals from the white noise behavior could be interpreted as a fault in the system.

In [30], signal-based and model-based fault detection schemes are compared to a flip-of-a-coin fault detector as applied to induction motor fault detection. The results of the study can be extended to centrifugal pump fault detection also. Receiver operating characteristic (ROC) curves are plotted for all the three types of detection schemes and their performances are compared with respect to the probability of false alarms and probability of fault detection. For false alarm rates of less than 50%, the flip-of-a-coin fault detector outperformed the signal-based detection scheme for the cases under consideration. It was possible to achieve 100% fault detection capability using the signal-based fault detection method, but at the same time there was a very high probability of false alarms (about 50%). On the contrary, the model-based fault detection method operated with 0% false alarm rates and had approximately 89% of fault detection capability. If the constraint on the false alarm probability was relaxed to about 10%, then it was possible to achieve 100% fault detection capability using the model-based detection technique.

C. The Basic Principle of Detecting Pump Faults Using Motor Electrical Signals

To obtain a better and an intuitive understanding of a fault detection method developed in this research, consider the system shown in Figure 9. The system under

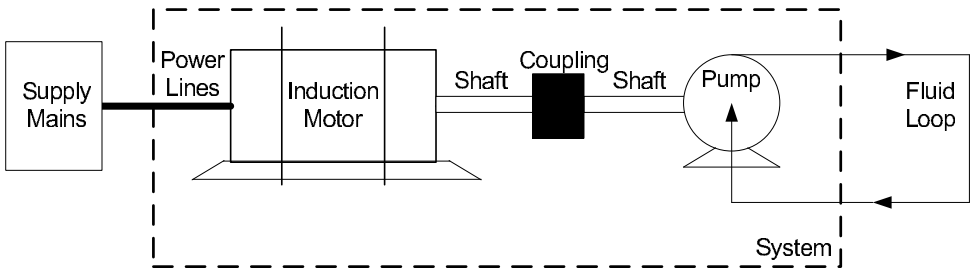

Fig. 9. Generalized system for pump fault detection.

consideration consists of a driver and a driven load. In this work, the driver is an induction motor and the driven load is a centrifugal pump. The pump is connected to the motor by means of a mechanical coupling. If the motor and the pump are both "healthy", then the system would perform as per the design specifications. The output of the motor, which is the torque produced, would be as expected. Similarly, the outputs of the pump, which are the flow rate and the pressure difference would be as per the characteristics curves of the pump provided by the manufacturer. However, if the motor is faulty then the output torque would not be the same as compared to a "healthy" motor and would have extra harmonics pertaining to the fault. Similarly, if the pump is not "healthy", then it would not be able to produce the required work horsepower. Moreover, the torque transmitted from the motor to the pump will also be influenced through the pump speed. Hence, a fault in either the pump or the motor will affect the torque produced by the induction motor. Any changes in the motor torque will be reflected as changes in the motor currents. Hence fault detection schemes based on analyzing the motor currents to detect centrifugal pump faults have

gained significant importance and attention over the last few years. In this study, the basic principle of model-based fault detection schemes previously used for detecting motor faults, is used in the development of techniques to detect pump faults.

Based on the above discussions, it can be concluded that a model-based fault detection scheme outperforms a signal-based fault detection schemes as regards to the generation of false alarms. The objective of this work is to develop a method that would be capable of detecting centrifugal pump faults with detection effectiveness of greater than 90% and 10% or lower rate of false alarms. Moreover, the use of sensors is to be avoided and only the motor electrical signals, which can be sampled using standard industrial installations, are to be used in the development of the method.

CHAPTER IV

PROPOSED FAULT DETECTION AND ISOLATION METHOD

A. Proposed Model-Based Fault Detection Scheme

The framework of the proposed model-based fault detection scheme is the same as that shown in Figure 8, except that the system under consideration is an induction motor-centrifugal pump system and the system model is empirically obtained. The flowchart for the proposed model-based fault detection method is shown in Figure 10.

The data acquisition block consists of sampling the motor electrical signals and vibration signals from the motor-pump system. The electrical signals (three phase currents and three line voltages) and the vibration signals (x, y and z-axis vibration signals) are sampled simultaneously, for comparison purposes.

The data preprocessing block includes downsampling the sampled signals to lower frequencies for further processing. The downsampled signals are further scaled to per-unit values. This demonstrates the feasibility of applying the fault detection algorithm to motor-pump systems of different power ratings and different make and manufacturers. In other words, since the fault detection method uses only the per unit values of the electrical signals, the algorithm can be applied to systems with any rated voltage and rated current. The scaling factors used to convert the signal to per-unit values are obtained during the training phase of the model development. Only the rated voltage, rated current and the CT and PT turn ratios are required to obtain these scaling factors. These constitute nameplate information and are easily accessible in most industrial facilities.

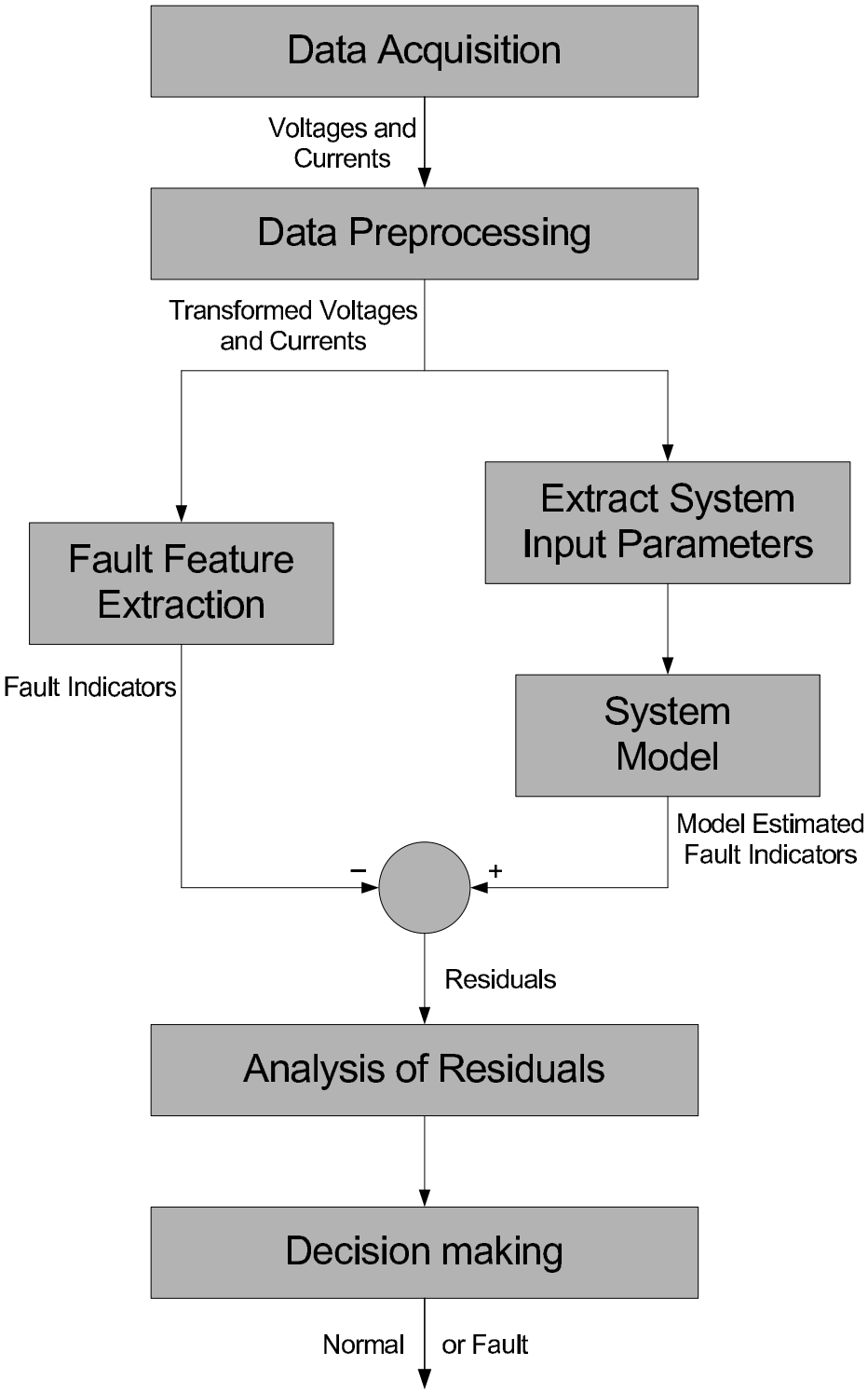

Fig. 10. Proposed model-based fault detection method.

1. Description of the Fault Detection Indicator

As mentioned earlier, any change in the system load would induce harmonic changes in the motor torque which would in turn induce harmonic changes in the motor current. Most of the available literature is based on extracting and tracking the variation of the characteristic frequency associated with a particular fault in the system. There are two main disadvantages associated with this approach. One is the fact that motor and/or pump design parameters or physical model parameters are required to obtain such characteristic frequencies. Secondly, owing to the non-stationary nature of the motor electrical signals, tracking one frequency component for fault detection would enable successful identification of the fault but this would also lead to the generation of large number of false alarms. To counter the above-mentioned drawbacks the proposed fault indicator is defined as follows:

$$\text{Fault Detection Indicator (FDI)} = \frac{1}{3}\sum_{a,b,c}\frac{\sum I_k^2}{I_f^2}, \tag{4.1}$$

where a,b and c are the three phases of the motor current, I_k is the RMS value of the k^{th} harmonic component in the motor current, I_f is the fundamental frequency component of the motor current and f_s is the sampling frequency of the signal.

2. Model Input Parameters

The inputs to the system model are various transformed signals computed from the raw voltages and raw currents such as voltage level, voltage imbalance, etc.

The voltage level is computed by obtaining the average of the voltage RMS of the three phases. The typical voltage level range is from 0.9 p.u. to 1.1 p.u., where 1.0 p.u. is the rated voltage level. The voltage RMS is computed using the formula

given below:

$$\text{Voltage RMS} = \sqrt{\frac{1}{N}\sum_{i=1}^{N} V_i^2}, \tag{4.2}$$

where V_i is the i^{th} sample of the voltage signal and 'N' is the total number of samples. *Overvoltage* is defined as an increase in the voltage level greater than 110% at the rated frequency for a duration longer than 1 minute. Similarly an *undervoltage* is a decrease in the voltage level to less than 90% at the rated frequency for a duration of longer than 1 minute. Overvoltages are usually due to load switching such as switching off a large load or energizing a capacitor bank. Overvoltages are caused because either the system is too weak to handle the desired voltage regulation or the voltage controls are inadequate. Undervoltages occur as a result of events that are opposite to the events causing overvoltages [31].

The average value of the motor current RMS over the three phases is also used as one of the inputs to the system model. The current RMS is computed using equation (4.2), except that V_i is replaced with I_i, which is the i^{th} sample of the motor current signal.

The typical voltage supply is usually well balanced in magnitude and phase. However, for many reasons, some degree of voltage imbalance occurs at the point of utilization that is varying with time. Voltage imbalance is the achilles heel of rotating equipment and even a slight degree of imbalance could harm a three-phase equipment operating at full capacity. The national electrical manufacturer's association (NEMA) defines voltage imbalance as the maximum deviation from the average of the three phase voltages divided by the average of the three phase voltages. Voltage imbalance, expressed in percent, is given as follows:

$$\text{Voltage Imbalance (\%)} = \frac{\max |V_X^{RMS} - V_{mean}^{RMS}|}{V_{mean}^{RMS}} \times 100, \tag{4.3}$$

where V_{mean}^{RMS} is the average of the three phase voltage and the subscript X stands for the three phases. The primary source of imbalance is the use of single phase loads on a three phase circuit. Voltage imbalance could also result from blown fuses. The impact of this problem is evident by the large industry in manufacturing of devices that monitor phase balance to protect motors. Any voltage imbalance of more than 5% is considered excessive.

Ideally, voltage and current waveforms must be perfectly sinusoidal in nature. However, due to the increase in electronic and other non-linear loads, these waveforms are distorted. This deviation from the ideal sine wave can be characterized by the spectral content of the deviation. There are basically four primary types of waveform distortion [31]:

- *DC Offset* - The presence of a dc voltage in an ac power system is termed as dc offset. This can occur as a result of asymmetry of electronic power converters. The presence of dc offset could be detrimental to transformer cores, as they might saturate in normal operation due to the unwanted bias present. This could further lead to additional heating and loss of transformer life.

- *Integer and Inter Harmonics* - Integer harmonics are sinusoidal voltages or currents having frequencies that are integer multiples of the fundamental frequency or the carrier frequency (usually 60 Hz). Interharmonics are those frequency components that are not integer multiples of the fundamental frequency. They can appear as discrete frequencies or as a wideband spectrum. The integer harmonics are due to the nonlinear characteristics of the devices and loads connected to the power system, whereas the sources of the interharmonic distortion are static frequency converters, induction motors, etc. Harmonic distortion levels in the signal can be characterized by means of a metric called the *total*

harmonic distortion (THD). The THD, expressed in percent, is given as

$$\text{Total Harmonic Distortion (THD) } (\%) = \frac{1}{V_f}\sqrt{\sum_{k>1}^{k_{max}} V_k^2} \times 100, \tag{4.4}$$

where V_f is the RMS value of the fundamental frequency component and V_k is the RMS value of the k^{th} harmonic component. Since the magnitude of the integer harmonics are much higher than that of inter-harmonics, a different metric must be used to characterize the amount of distortion caused only by the inter-harmonics.

- *Notching* - Notching is defined as the periodic voltage disturbances caused by the normal operation of power electronic devices when current is commutated from one phase to another. Since notching occurs continuously, it can also be characterized through the harmonic spectrum of the voltage. The frequency components of notching are very high.

- *Noise* - Noise is defined as unwanted electrical signals with broadband spectral content lower than 200 kHz. These are superimposed upon the power system voltage or current phase conductors or found on neutral conductors or signal lines .

The signals are unbiased to remove the dc offset and are downsampled to lower frequencies to remove the effect of notching (if present) and high frequency noise.

3. Development of the Predictive Model

As described in the previous section, the model describes a relation between the baseline (or "healthy") response of the system and the various system inputs. In other words, the model relates the time varying fault indicator as a function of the

time varying system inputs. The model structure can be expressed as

$$\text{FDI(k)} = f(u_i(k), u_i(k-1), ..., u_i(k-n)); \qquad i = 1, ..., N \tag{4.5}$$

where "$f(.)$" is the unknown function to be modeled, u(.) are the time series of the inputs, n is the net delay in the inputs, k is the discrete-time and N is the number of inputs used.

In this study, the function "$f(.)$" is modeled as a polynomial of the various inputs taking the form of a polynomial NARX. The model parameters of the function "$f(.)$" are to be estimated online during commissioning.

The accuracy of the model output depends on the nature (accuracy, volume, etc) of the raw data used in the training or estimation phase. Hence the system is operated in a sufficiently wide range to cover the entire operating envelope of interest. The proposed model is developed using data collected from the baseline system. The developed model predicts the baseline fault indicator estimate for a given operating condition characterized by the model inputs. The model is validated using data that are different from the one used in its development. The model prediction error is defined as

$$\text{Error } (\%) = \frac{|y_i - \hat{y_i}|}{\sqrt{\sum_{i=1}^{N} y_i^2}} \times 100; \qquad i = 1, ..., N. \tag{4.6}$$

where y_i is the measured variable and $\hat{y_i}$ is the model predicted variable. Figure 11 and Figure 12 show the histogram of the prediction errors of the model at 20% and 40% of the rated load level, respectively.

No fault data are used to train the model. Hence for anomalies in the pump or motor, the output of the model will be the system baseline fault indicator for the given operating condition. No motor or pump design parameters are used in the development of the baseline model. Hence this model can be easily ported to other

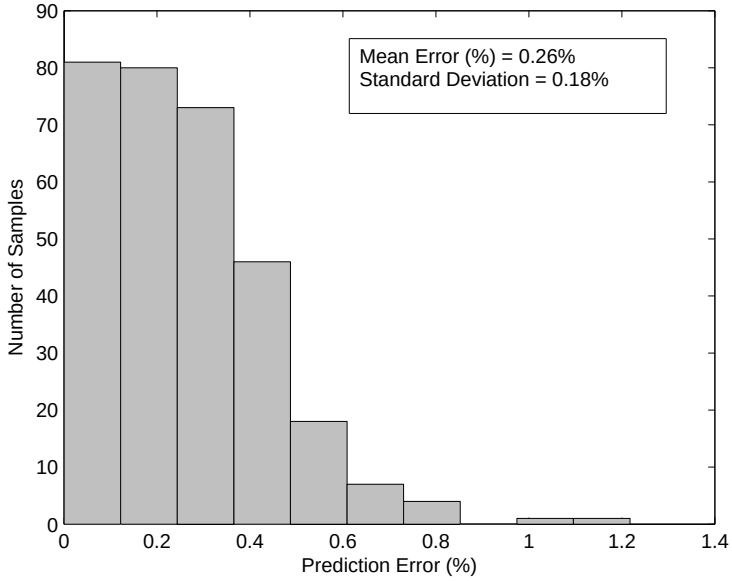

Fig. 11. Histogram of model prediction error at 20% of rated load level.

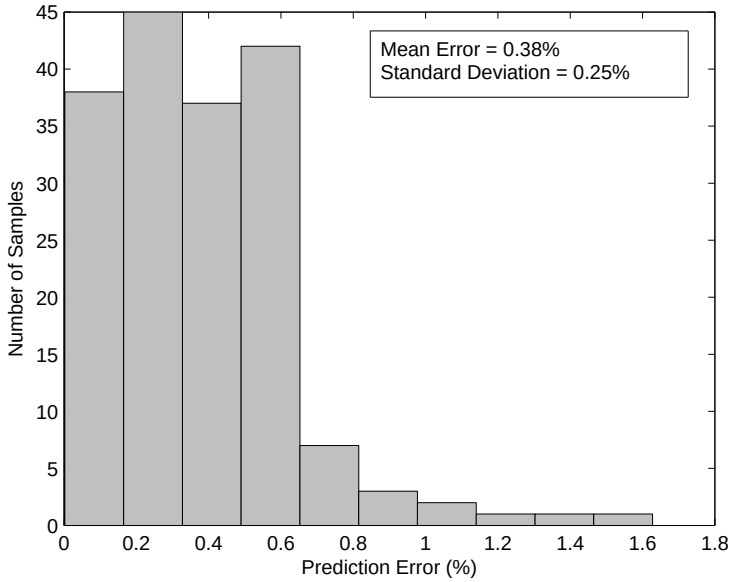

Fig. 12. Histogram of model prediction error at 40% of rated load level.

motor-centrifugal pump systems, as only the measured motor voltages and currents are used in model development. However, each motor-centrifugal pump system will have a different baseline model, which can be adaptively developed using the measured motor electrical signals.

4. Decision Making

The model predicted output is compared to the FDI extracted from the measured signals and the residuals between the two are computed. If the system is "healthy", then the residual signal would be closed to a white noise signal. However, if there is a fault in the system, then the residual will deviate from the white noise behavior. If this deviation exceeds a certain threshold then a "fault" alarm is issued. Otherwise, the system is considered "healthy" and the procedure is repeated. If the detection threshold is chosen to be large, then although the false alarm rates are reduced, there is a very high probability of missing a fault. Similarly, if the detection threshold is chosen very small then along with good fault detection capability, there is a very high probability of generating false alarms. Hence a balance has to be achieved in deciding the detection threshold. One factor in choosing the threshold is the intended application of the detection method or the system that is being monitored. For example, in space applications a high rate of false alarms is acceptable as people's life are at stake. Hence the threshold can be chosen small to detect any anomaly. In utility industries however, false alarms are not tolerated and hence a somewhat higher threshold is preferred. The detection method might not detect the fault as soon as the fault initiates, but might detect it as the fault degrades and well before any catastrophic failure.

B. Proposed Model-Based Fault Isolation Scheme

The output of the model developed in the previous section is affected by either a fault in the induction motor or a fault in the centrifugal pump or any other component affecting the motor output. For the purpose of this study only motor and pump faults are assumed. Hence, it is not possible to isolate a developing fault. To distinguish between faults in the motor and faults in the pump, a localized model of one of the components is required wherein the output of the model is affected only by the faults in that component and is insensitive to the faults in the other. In this study, since no measurement is available from the centrifugal pump, a localized model for the induction motor is developed. The output of this model is only sensitive to faults in the motor and is insensitive to faults in the centrifugal pump. Figure 13 shows the overall schematic of the proposed fault detection and isolation method. The fault isolation method is used to distinguish between motor and pump faults only when a fault within the system is detected. If the system is "healthy", then the next data set is analyzed to check for the presence or lack of fault and the fault isolation method is not used.

1. Development of the Localized Induction Motor Model

Consider an induction machine such that the stator windings are identical, sinusoidally distributed windings, displaced by 120^o, with N_s equivalent turns and resistance, r_s. Consider the rotor windings as three identical sinusoidally distributed windings displaced by 120^o, with N_r equivalent turns and resistance, r_r. The voltage equations are given as

$$v_{abcs} = r_s i_{abcs} + p\lambda_{abcs} \tag{4.7}$$

$$v_{abcr} = r_r i_{abcr} + p\lambda_{abcr} \tag{4.8}$$

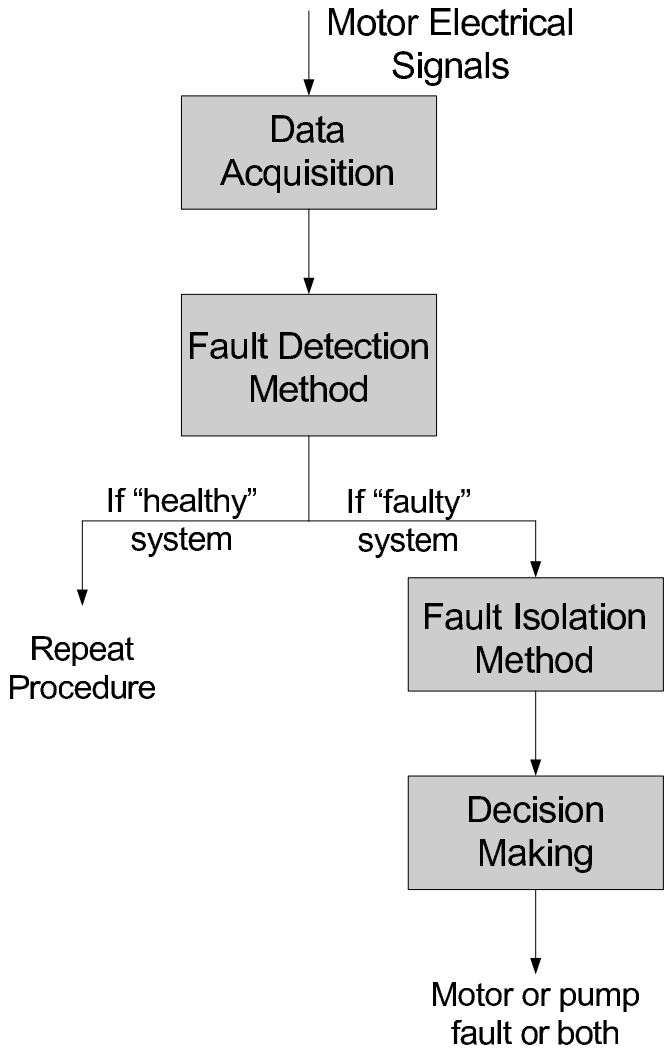

Fig. 13. Overall schematic of proposed fault detection and isolation method.

where p is the first derivative operator, subscript s denotes variables and parameters associated with stator circuits, subscript r denotes the variables and parameters associated with the rotor circuits. r_s and r_r are diagonal matrices each with equivalent nonzero elements and

$$\begin{aligned}(f_{abcs})^T &= [f_{as} \quad f_{bs} \quad f_{cs}] \\ (f_{abcr})^T &= [f_{ar} \quad f_{br} \quad f_{cr}]\end{aligned} \tag{4.9}$$

where f represents either voltage, current or flux linkages.

For a magnetically linear system, the flux linkages may be expressed,

$$\begin{bmatrix} \lambda_{abcs} \\ \lambda_{abcr} \end{bmatrix} = \begin{bmatrix} L_s & L_{sr} \\ L_{sr}^T & L_r \end{bmatrix} \begin{bmatrix} i_{abcs} \\ i_{abcr} \end{bmatrix}, \tag{4.10}$$

where L_s and L_r are the winding inductances which include the leakage and magnetizing inductances of the stator and rotor windings, respectively. The inductance L_{sr} is the amplitude of the mutual inductances between the stator and rotor windings. L_s and L_r are constants and L_{sr} is a function of the mechanical rotor position, $\theta_m(t)$. Details of the variables are described in [32].

The vast majority of induction motors used today are singly excited, wherein electric power is transformed to or from the motor through the stator circuits with the rotor windings short-circuited. Moreover, a vast majority of single-fed machines are of the squirrel-cage rotor type. For a squirrel cage induction motor, $v_{abcr} = 0$. Substituting equation (4.10) into equations (4.7) and (4.8), we get,

$$v_{abcs} = r_s i_{abcs} + L_s(pi_{abcs}) + (pL_{sr})i_{abcr} + L_{sr}(pi_{abcr}), \tag{4.11}$$

$$0 = r_r i_{abcr} + (pL_{sr}^T)i_{abcs} + L_{sr}^T(pi_{abcs}) + L_r(pi_{abcr}). \tag{4.12}$$

At steady-state, equations (4.11) and (4.12) can be expressed as,

$$\tilde{V}_s(t) = (r_s + j\omega_s L_s)\tilde{I}_s(t) + (j\omega_s L_{sr})\tilde{I}_r(t), \tag{4.13}$$

$$0 = j\omega_r L_{sr}^T \tilde{I}_s(t) + (r_r + j\omega_r L_r)\tilde{I}_r(t). \tag{4.14}$$

The detailed derivation can be found in [32].

In equation (4.14), assuming that $(r_r + j\omega_r L_r)$ is invertible, $\tilde{I}_r(t)$ can be expressed as,

$$\tilde{I}_r(t) = -\frac{j\omega_r L_{sr}^T}{r_r + j\omega_r L_r}\tilde{I}_s(t). \tag{4.15}$$

Substituting equation (4.15) into equation (4.13), we have,

$$\tilde{V}_s(t) = (r_s + j\omega_s L_s + \frac{\omega_s \omega_r L_{sr} L_{sr}^T}{r_r + j\omega_r L_r})\tilde{I}_s(t). \tag{4.16}$$

Assuming $(r_s + j\omega_s L_s + \frac{\omega_s \omega_r L_{sr} L_{sr}^T}{r_r + j\omega_r L_r})$ is invertible, the following relationship between stator voltages and currents can be obtained,

$$\tilde{I}_s(t) = [r_s + j\omega_s L_s + \frac{\omega_s \omega_r L_{sr} L_{sr}^T}{r_r + j\omega_r L_r}]^{-1}\tilde{V}_s(t). \tag{4.17}$$

$$\tilde{I}_s(t) = [Z]^{-1}\tilde{V}_s(t). \tag{4.18}$$

where Z is a function of the machine parameters which in turn are functions of the mechanical rotating angle of the rotor, $\theta_m(t)$. Equation (4.18) represents a modulator wherein the current spectrum will be composed of both the input voltage frequencies and also other frequency components due to the modulation. The modulated frequencies will appear as side-bands in the current spectrum around each frequency component corresponding to the input voltage signal. Hence an induction motor can be generalized as a modulator as shown in Figure 14, where U(n) is the system input, the stator voltages, A(n) is the signal containing the spatial harmonics of the motor and Y(n) is the system output, the stator currents.

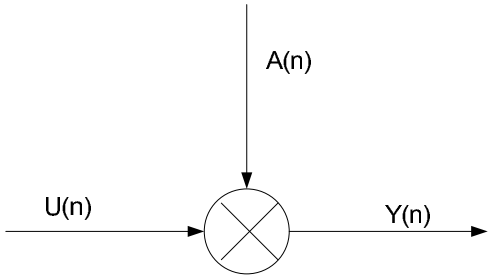

Fig. 14. Induction motor modulator model.

Any fault in the rotor of the induction motor or in the motor bearings would result in the generation of additional spatial irregularities. This would induce additional spatial harmonics in the motor air-gap flux. These additional harmonics would modulate the voltage frequencies and appear as sidebands in the stator current spectrum. Higher order spectra are used to detect these modulated frequencies in the stator current spectrum.

2. Use of Higher Order Spectra Analysis

Higher-order spectra is a rapidly evolving signal processing area with growing applications in science and engineering. The power spectral density or the power spectrum of deterministic or stochastic processes is one of the most frequently used digital signal processing technique. The power spectrum estimation methods can be classified into a number of different categories, namely, maximum-likelihood methods, maximum-entropy methods, harmonic decomposition methods, etc. In power spectrum estimation, the process under consideration is treated as a superposition of statistically uncorrelated harmonic components and the distribution of power among these frequency components is then estimated. The phase relationships between frequency components are suppressed. The information contained in the power spectrum is essentially present in the autocorrelation sequence. This is sufficient for the com-

plete statistical description of a Gaussian process of known mean. However, there are practical situations where the power spectrum or the autocorre1ation domain is not sufficient to obtain information regarding deviations from Gaussianness and the presence of nonlinearities in the system that generates the signals. Higher order spectra (also known as polyspectra), defined in terms of higher order cumulants of the process, do contain such information. Particular cases of higher order spectra are the third-order spectrum also called the bispectrum, defined as the Fourier transform of the third-order cumulant sequence of a stationary random process, and the trispectrum (fourth-order spectrum), which is the Fourier transform of the fourth-order cumulant sequence of a stationary random process. The power spectrum is, in fact, a member of the class of higher order spectra, i.e., it is the second-order spectrum [33].

The main reasons for using higher order spectral analysis in signal processing are itemized below [33]:

- to suppress Gaussian noise processes of unknown spectral characteristics in detection, parameter estimation and classification problems; the bispectrum also suppresses non-Gaussian noise with symmetrical probability density function (pdf),
- to reconstruct the phase and magnitude response of signals or systems, and
- to detect and characterize the nonlinearities in time series.

In this study higher order spectra are used to detect the phase relationship between harmonic components that can be used to detect motor related faults. One of the most widely used method in detecting phase coupling between harmonic components is the bispectrum estimation method. In fact, bispectrum is used in detecting and characterizing quadratic phase coupling.

Consider a discrete, stationary, zero-mean random process, *x(n)*. The bispectrum of *x(n)* is defined as

$$B(\omega_1, \omega_2) = \sum_{\tau_1=-\infty}^{\infty} \sum_{\tau_2=-\infty}^{\infty} c(\tau_1, \tau_2) \exp[-j(\omega_1 \tau_1 + \omega_2 \tau_2)], \tag{4.19}$$

where,

$$c(\tau_1, \tau_2) = E[x(n)x(n+\tau_1)x(n+\tau_2)], \tag{4.20}$$

where $E[.]$ denotes the expectation operator. A class of techniques named "direct" can be used to estimate the bispectrum. This technique uses the discrete fourier transform (DFT) to compute the bispectrum as follows:

$$B(k_1, k_2) = E[X(k_1)X(k_2)X^*(k_1 + k_2)], \tag{4.21}$$

where $X(k)$ is the DFT of $x(n)$.

From equation (4.21), it can be concluded that the bispectrum only accounts for phase couplings that are the sum of the individual frequency components. However, motor related faults manifest themselves as harmonics that modulate the fundamental frequency and appear as sidebands at frequencies given by $|f_e \pm m f_v|$, where f_e is the fundamental frequency and f_v is the fault frequency. Hence, the bispectrum estimate given by equation(4.21) detects only half of the coupling, as it does not detect the presence of the other half given by the difference of the two frequency components. Moreover, information about the modulation frequency has to be known to use this bispectrum estimate correctly. This point can be illustrated with the following example. Consider the following two signals,

$$x_1(n) = \cos(2\pi 60n + \phi_1) \tag{4.22}$$

$$x_2(n) = B + \cos(2\pi 20n + \phi_2) \tag{4.23}$$

where, ϕ_1 and ϕ_2 are arbitrary phase angles. The signal, $x_1(n)$ is considered to be an unbiased signal as is the case in power system applications. In this example, $x_1(n)$ is analogous to the carrier signal and $x_2(n)$ is analogous to the signal that modulates the carrier signal. The product of these two signals results in,

$$\begin{aligned} x(n) &= x_1(n)x_2(n) \\ &= B\cos(2\pi 60n + \phi_1) + \cos(2\pi 60n + \phi_1)\cos(2\pi 20n + \phi_2) \\ &= B\cos(2\pi 60n + \phi_1) + \frac{1}{2}\cos(2\pi 80n + \phi_1 + \phi_2) \\ &\quad + \frac{1}{2}\cos(2\pi 40n + \phi_1 - \phi_2). \end{aligned} \tag{4.24}$$

For simplicity, the constant B is assumed to be equal to 1. In the resultant signal, the 40Hz and the 80Hz components are obtained due to the modulation of the 20Hz component with the 60Hz carrier frequency. From equation (4.21), it can be concluded that for the bispectrum to correctly identify this modulation relationship, the carrier frequency and the modulation frequency information have to be known. However, in the example shown above, the final signal *x(n)*, does not contain any information about the modulation frequency. Hence the bispectrum cannot be used to correctly identify the modulation relationship as is evident from Figure 15. The bispectrum plot is typically displayed as a three-dimensional plot with frequency on the x and y axes and the magnitude on the z axis. For simplicity, this study uses two-dimensional contour plots with frequency on the x and y and the magnitude coming out of the page. Figure 15 shows a peak at frequency pair (40Hz, 40Hz), indicating that the signal is made up of only 40Hz frequency component and that 40Hz is the modulation frequency, which is not the case. Hence to correctly identify the modulation relationship, a modified bispectrum estimator is used [34].

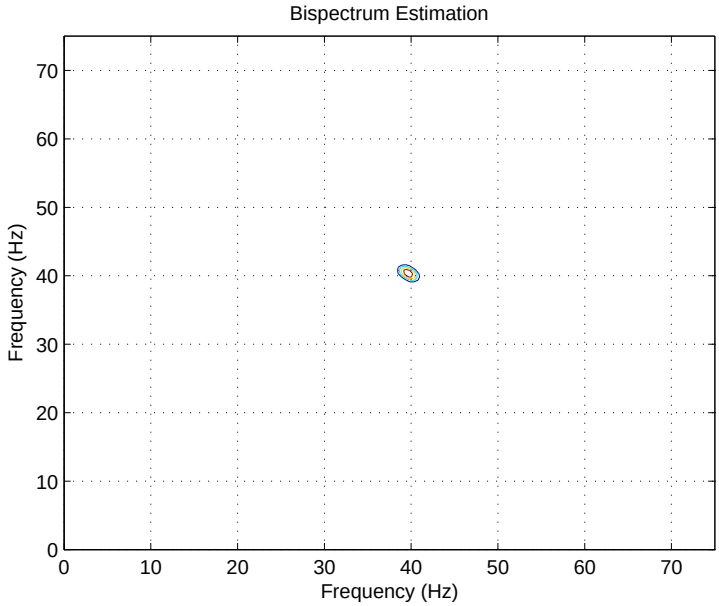

Fig. 15. Modulation frequency detection using bispectrum.

3. Description of the Fault Isolation Indicator

The modified bispectrum estimator also referred to as the amplitude modulation detector (AMD) is defined as follows:

$$\widehat{AMD}(k_1, k_2) = E[X(k_1 + k_2)X(k_1 - k_2)X^*(k_1)X^*(k_1)]. \tag{4.25}$$

From equation (4.25), it can be seen that both the sidebands of the modulation are accounted for in the definition. Figure 16 shows the modified bispectrum for the example considered in the previous subsection. The peak at the frequency pair (60Hz, 20Hz) indicates that the 20Hz frequency component modulates the 60 Hz frequency component. Moreover, no information about the modulation frequency is utilized in computing the modified bispectrum. This is very useful since the motor related fault frequencies which modulate the supply frequency are very difficult to

compute. These frequencies are dependent on the design parameters, which are not easily available. For example, the fault frequency pertaining to a motor rolling element bearing depends on the number of balls in the bearing, the ball diameter, the pitch diameter, etc. Hence it is desirable to design an algorithm which does not require the motor design parameters. Therefore, in this study, various forms of the AMD indicator depicted in equation(4.25) are used to detect motor related faults.

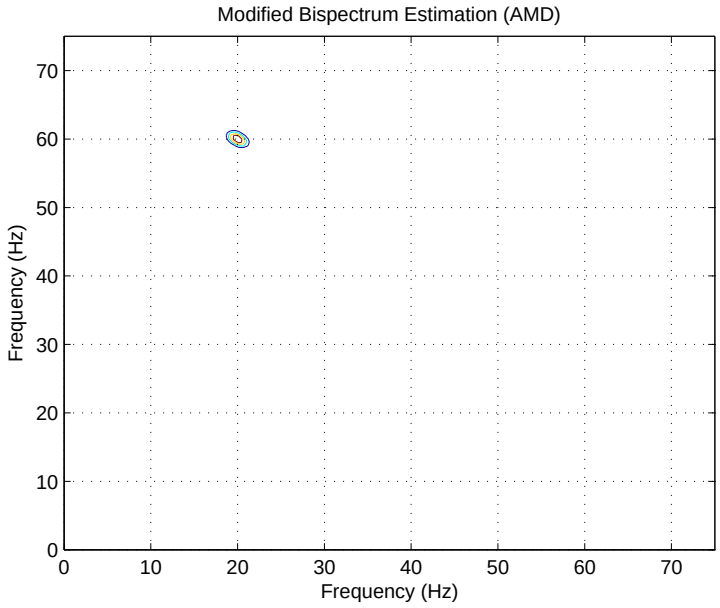

Fig. 16. Modulation frequency detection using the modified bispectrum or the amplitude modulation detector.

The reason that the AMD correctly identifies the modulation relationship is that it detects phase coupling. If phase coupling exists between frequency components, then the AMD component at those frequencies will have zero phase and maximum peak. To illustrate this, consider the equation (4.25) and represent it in terms of its

phase and magnitude, as follows:

$$E[|X(k_1+k_2)|e^{j\angle(k_1+k_2)}|X(k_1-k_2)|e^{j\angle(k_1-k_2)}|X^*(k_1)|e^{-j\angle(k_1)}|X^*(k_1)|e^{-j\angle(k_1)}] \quad (4.26)$$

Rearranging the terms results in,

$$E[|X(k_1+k_2)||X(k_1-k_2)||X^*(k_1)||X^*(k_1)|e^{j(\angle(k_1+k_2)+\angle(k_1-k_2)-\angle(k_1)-\angle(k_1))}]. \quad (4.27)$$

If there is phase coupling between the frequency components k_1 and k_2, then

$$\angle(k_1+k_2) = \angle(k_1) + \angle(k_2), \text{ and} \quad (4.28)$$

$$\angle(k_1-k_2) = \angle(k_1) - \angle(k_2). \quad (4.29)$$

Substituting equations (4.28) and (4.29) in equation (4.27), results in zero phase and the final expression is the expectation of the product of the magnitudes. Hence, if the frequency components, k_1, k_1+k_2 and k_1-k_2 exists in the spectrum, and if there is phase coupling between the frequency components, k_1 and k_2, then the detector will exhibit a peak at $AMD(k_1, k_2)$, indicating that frequencies k_1 and k_2 are modulated components.

The AMD spectrum is a two dimensional matrix. The frequency resolution of AMD can be calculated by $\Delta f = \frac{f_s}{N}$ [33], where f_s is the sampling frequency and N is the total number of samples. A good frequency resolution will lead to a large AMD matrix, which cannot be implemented easily and would require large memory and a very fast processor. In this study, we are interested only in the frequency components that are modulated with one specified frequency; for example, the supply fundamental frequency. Therefore, it is possible to use only a one dimensional AMD, to calculate the AMD spectra that are modulated only with the supply fundamental frequency.

The induction motor has been modelled as the modulator shown in Figure 14.

Any fault in the rotor or the motor bearings would lead to the generation of spatial harmonics which modulate the frequencies corresponding to the input voltage and manifest as sidebands in the motor current. Since the spatial harmonics pertaining to the fault are unknown, the AMD is used to detect if any such modulation relationship exists, which does not require any information about the modulation frequency component. Detailed derivations of these AMD indicators are given in [35].

C. Vibration-Based Signal Analysis

The effectiveness of the model-based scheme is compared to the effectiveness of a continuous vibration monitoring scheme. A tri-axial accelerometer is mounted on top of the pump to continuously monitor the vibration level of the pump, both during the normal operation and during the staged fault experiments. Similarly, an accelerometer is mounted on the motor close to the bearing housing to monitor the change in the vibration level as the motor bearing condition degrades. The vibration levels in the x, y and z directions are recorded and the aggregate vibration level is used as an indicator to detect the presence of a fault. The indicator is defined as follows:

$$\text{Vibration Indicator (VI)} = \frac{1}{3}\sum_{x,y,z}\sqrt{\frac{1}{N}\sum_{i=1}^{N} Vib_{X,i}^2} \tag{4.30}$$

where $Vib_{X,i}$ is the i^{th} sample of the vibration signal in the X direction, where X stands for the three axes *x, y, z*, and N is the total number of samples. Since the vibration level of the system varies after each re-assembly and cannot be controlled, a fixed threshold cannot be used for detection. Hence, an adaptive threshold is used. In this study, a multiple of the standard deviation of the baseline vibration is used as the detection threshold.

CHAPTER V

EXPERIMENTAL RESULTS

A. Description of the Experimental Setup

A schematic diagram of the experimental setup used in this research is shown in Figure 17. The experimental setup consists of a centrifugal pump driven by a $3-\phi$, 2 pole, 3 hp induction motor energized by constant frequency voltage from the power mains. A variable height reservoir is used as the suction and discharge sump and the height of the reservoir can be varied so as to increase or decrease the load on the motor. Pressure gauges are mounted on the suction and discharge side of the pump along with a flow meter to obtain the characteristic curves of the centrifugal pump. A throttle valve is located on the suction side of the pump. The valve position is varied to stage cavitation problems in the centrifugal pump. Similarly, a pneumatically controlled valve is located on the discharge side of the pump. This valve position is changed to increase or decrease the flow rate of the pump, which in turn results in the increase or decrease of the load on the motor. A triaxial accelerometer is placed on the pump housing close to the eye of the impeller and one on top of the motor bearing housing, to measure the vibration level of the pump and the motor. The motor line voltages and phase currents are measured using potential transducers (PT) and current transducers (CT), respectively. The output signals from these sensors are passed through a signal conditioning unit that anti-aliases the signals using an eighth order elliptic filter. A 16-channel $LabVIEW^{TM}$ data acquisition system is used to record the three line voltages, the three phase currents and the six vibration signals. Figure **??** shows the photograph of the experimental setup used in this research.

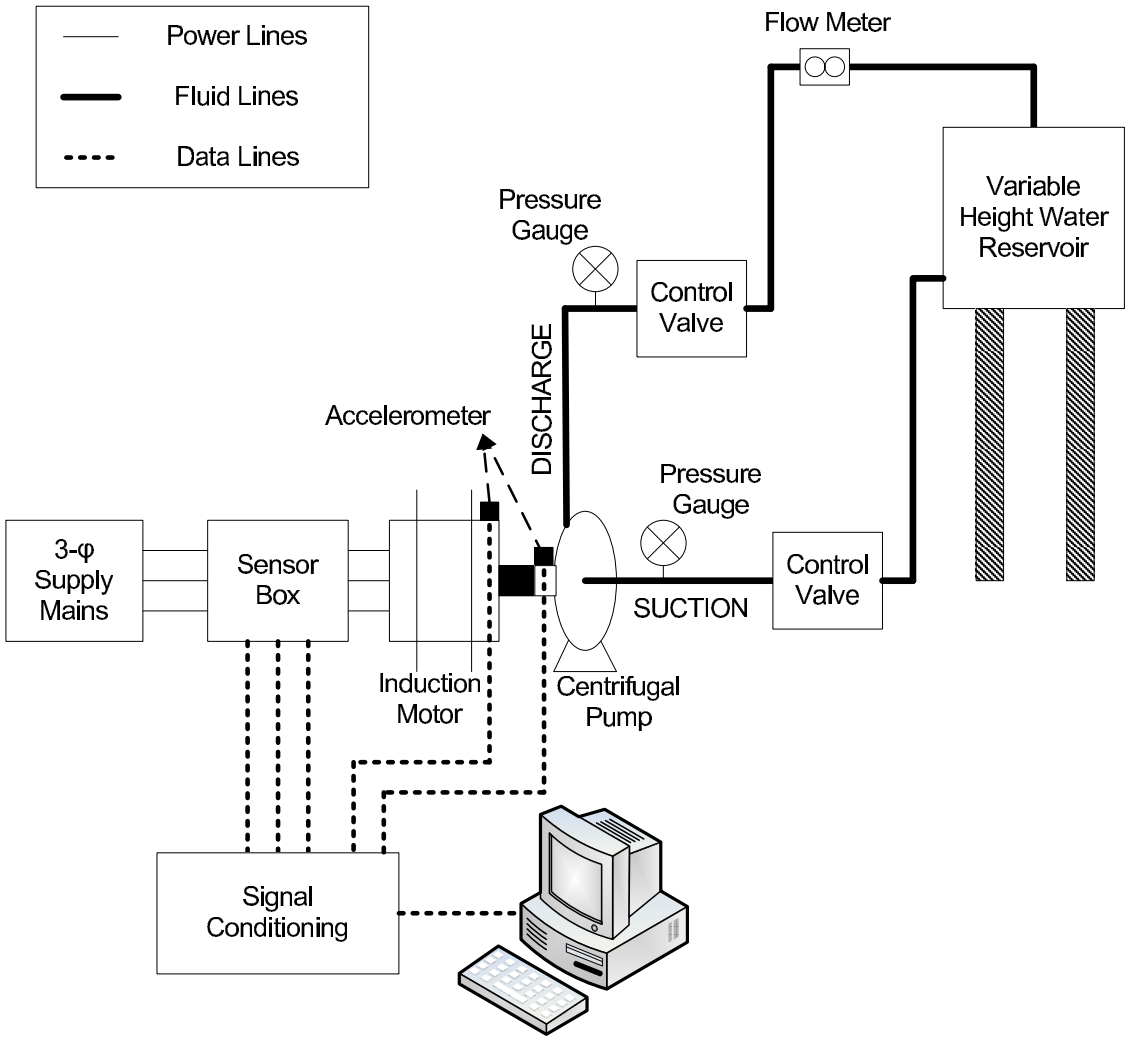

Fig. 17. Schematic of the motor-pump-fluid loop experimental setup.

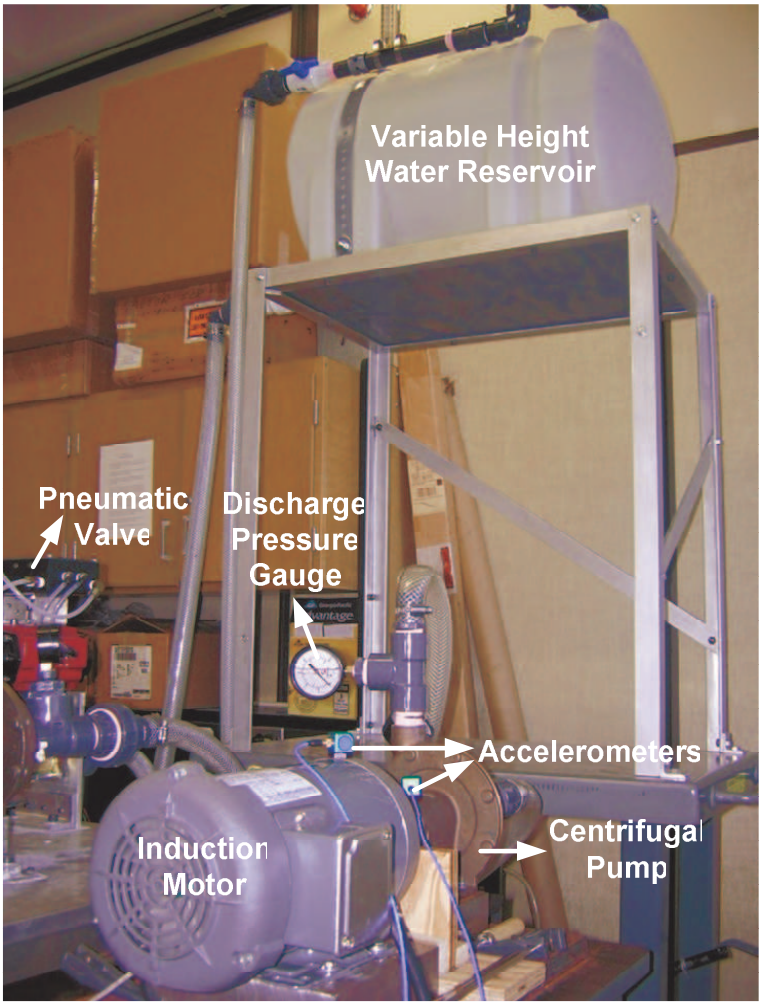

Fig. 18. Photograph of the motor-pump-fluid loop experimental setup.

B. "Healthy" Pump Experiments

Experiments are first conducted to validate the effectiveness of the proposed fault detection scheme in generating low rates of false alarms. The experiments with a "healthy" pump are run for about 100 hours over a period of 12 days. In these experiments, the motor is considered to be "healthy" as well. Different loading conditions are also staged to test the performance of the proposed fault detection method in recognizing the change in the load. Data from these experiments are used to analyze the false alarms generated by the detection system. Over $15 - 20$ case studies are actually conducted to obtain statistically significant results. A couple of cases are shown to illustrate the performance effectiveness of the proposed method in not generating a false alarm when the system is "healthy". Figure 19 and Figure 20 show the fault detection indicator change (FDIC) with respect to the baseline, for a "healthy" system when the load on the motor is about 20% and 40% of rated value, respectively. Note that the FDIC is below the threshold, as expected.

1. Impact of Power Quality Changes

As mentioned in the previous chapter, motor currents are affected not only by the faults in the system, but also by changes in the power supply and load. In industrial environments, the input voltages to a motor are affected by other equipment connected to the same voltage bus. Many equipments inject a lot of harmonics into the bus, which affects the motor stator voltages and currents in an unpredictable manner. Experiments are conducted to study the effect of harmonic distortion on the detection capability of the proposed method. In these experiments, the motor-pump system is "healthy" and the load on the motor is approximately 45% of the rated value. Table II lists sample test results of an experiment, which is conducted to study the

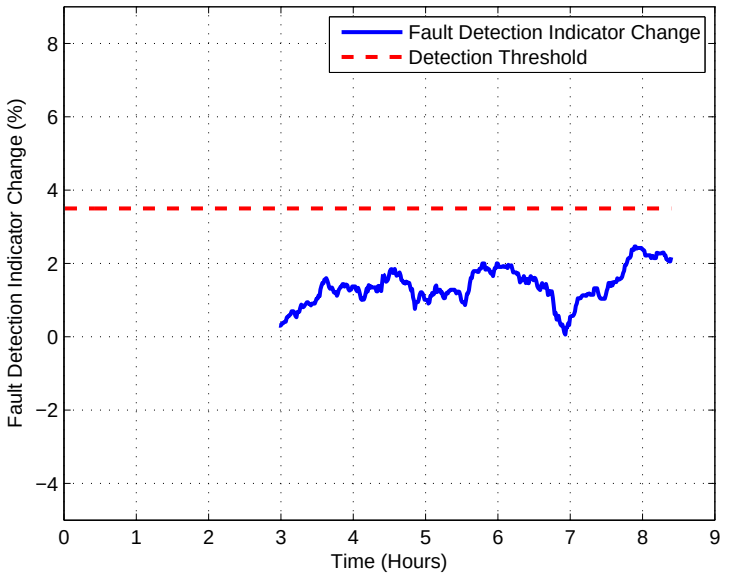

Fig. 19. Proposed FDIC at 20% of rated load.

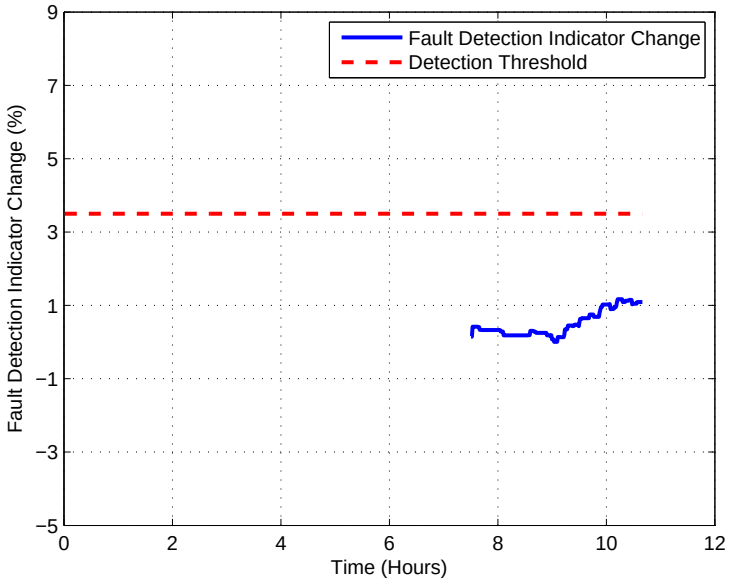

Fig. 20. Proposed FDIC at 40% of rated load.

Table II. Motor input voltage parameters.

Data Set No.	Average Voltage RMS (p.u.)	Average Current RMS (p.u.)	Average Voltage Imbalance (%)	Average Voltage THD (%)	Average Voltage NSR (%)
1	0.9912	0.4455	0.573	2.569	0.000624
2	0.9912	0.4453	0.560	2.567	0.000574
3	0.9911	0.4462	0.563	2.559	0.001057
4	0.9910	0.4464	0.568	2.545	0.002267
5	0.9908	0.4458	0.574	2.573	0.000650
6	0.9908	0.4461	0.563	2.568	0.000936
7	0.9904	0.4455	0.552	2.561	0.000653
8	0.9904	0.4454	0.554	2.564	0.000706
9	0.9928	0.4456	0.561	2.564	0.002936
10	0.9924	0.4458	0.566	2.552	0.004013

effects of noise related harmonics found in motor voltages. The 10 data sets shown are collected over a period of 1 hour. The experimental results show that the average values of the voltage RMS, current RMS, voltage imbalance and voltage THD do not vary much, but the average voltage noise-to-signal ratio (NSR) varies by about 600%. This variation in the NSR results in harmonic changes in the motor currents, which in turn leads to the generation of false alarms. This is illustrated in Figure 21. The top portion of the figure shows the FDIC with respect to the baseline without taking into account the changes in the power quality. This shows the existence of a fault, thereby generating a false alarm. The bottom portion of the figure shows the FDIC for the same case, but this time the proposed model-based detection scheme is

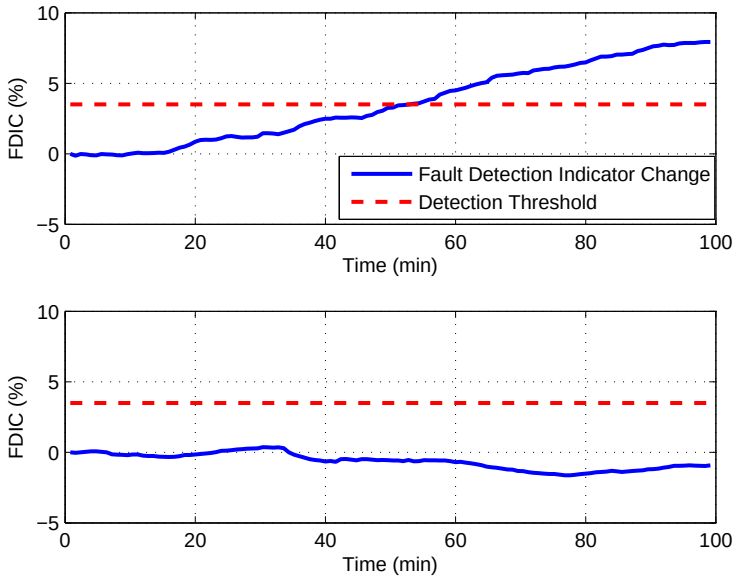

Fig. 21. Power quality variations; FDIC without considering power supply distortion changes (top); Proposed FDIC with proposed model-based fault detection approach (bottom).

used. This results in the FDIC remaining well below the detection threshold, thereby avoiding any false alarm.

2. Impact of Load Variations

Load changes induce changes in the harmonics of the motor current, which can be similar to certain fault induced harmonics. Experiments with only load changes without any power supply variations, are difficult to stage, because our laboratory is not equipped to control power supply variations. Hence experiments with both power supply variations and load changes are staged to study their effects on the motor currents. Figure 22 shows the voltage spectrum of two different data sets, one at 20% of the rated load level and the other at 40% of the rated load level. The motor and the pump are both "healthy". It can be seen that there is very little variation or

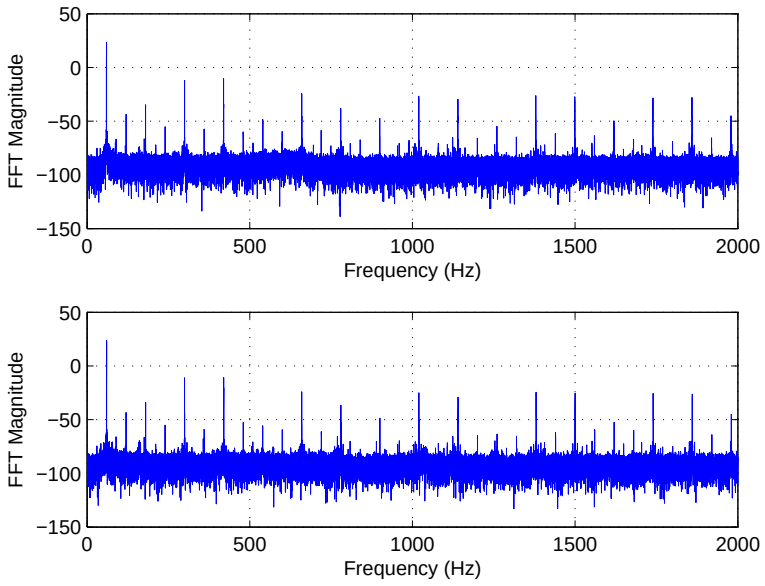

Fig. 22. Voltage spectra; 20% rated load level (top); 40% rated load level (bottom).

difference in the two spectra. However, in Figure 23, which shows the current spectra for the same two data sets, there is a significant amount of difference between the two. Note that the current spectrum at 40% rated load level has more harmonics than the spectrum at 20% rated load level. Hence, if one were to just analyze the current spectrum for changes, then this would look like a fault but in reality this change in the harmonic content is only a manifestation of the load change and some slight variations in the power quality.

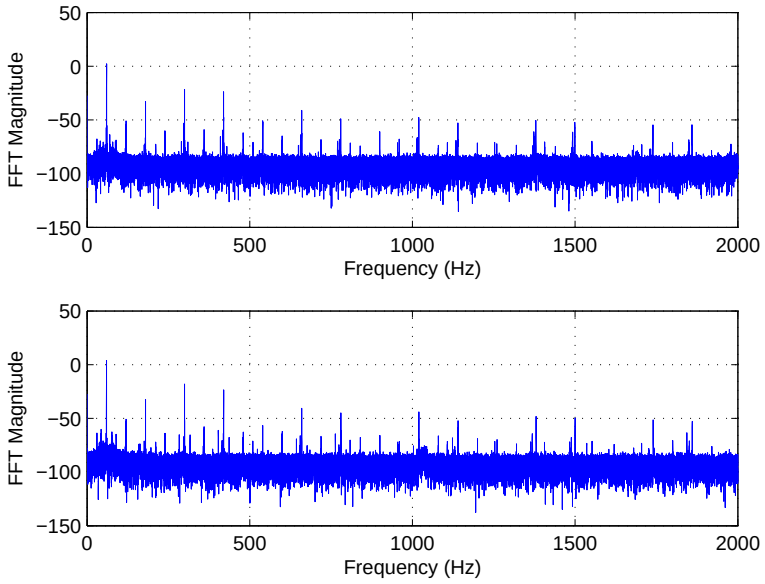

Fig. 23. Current spectra; 20% rated load level (top); 40% rated load level (bottom).

This is more clearly illustrated in Figure 24, which shows the combined effects of load variations and power quality changes on the FDIC. The top portion of the figure shows the FDIC when these operating condition changes are not accounted for. This shows the existence of a fault, which is a false alarm. The bottom portion of the figure shows the FDIC if the proposed model-based detection scheme is applied

to the same case. In this case, the FDIC is below the detection threshold thereby avoiding the generation of a false alarm.

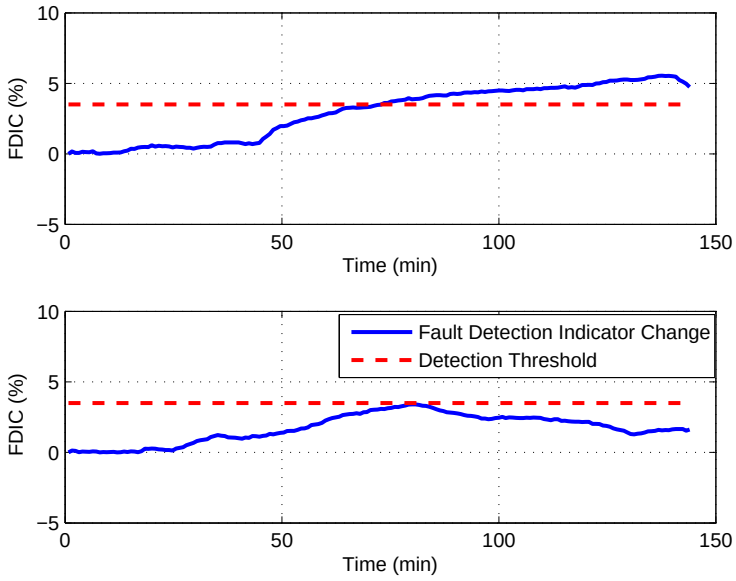

Fig. 24. Load and power supply variations; FDIC without considering load and power supply variations (top); Proposed FDIC with proposed model-based fault detection approach (bottom).

C. Staged Pump Fault Experiments

Once the effectiveness of the model-based fault detection scheme in reducing false alarms is established, experiments are conducted to validate the detection effectiveness of the proposed scheme. Three different failure modes of centrifugal pumps, namely, cavitation, damaged impeller and damaged bearing, are staged to validate the performance of the proposed model-based fault detection algorithm in detecting the presence of a fault. Each staged pump failure mode is described in some detail in the following subsections.

1. Pump Cavitation

Cavitation is defined as the formation and subsequent collapse or implosion of vapor bubbles in the pump. Cavitation occurs because the absolute liquid pressure falls below the liquid's vapor pressure. When cavitation occurs in a pump, its efficiency is reduced. If the pump operates under cavitation conditions for sufficiently long period, then this could lead to premature bearing and seal failure.

In this study, the severity of cavitation experienced by the pump is quantified by means of suction pressure measurements. The suction pressure is varied by throttling the flow at the suction side of the pump to create cavitation in the pump. There are two ways by which it is determined that the cavitation is in fact occurring and that it is occurring at the impeller. One is the generation of the rattling sound at the eye of the impeller when the cavitation experiments are conducted. The second is through measurements and analysis of the vibration signal. Since the triaxial accelerometer is placed near the eye of the impeller, any change in the vibration level would indicate the presence of cavitation at the impeller rather than at the elbows or the valve. Three different cavitation levels are staged with each level experiencing more severe cavitation than the previous one. Table III summarizes the three levels of the cavitation with respect to the suction pressure.

Extensive experiments have been conducted to verify the fault detection effectiveness of the proposed system. The experiments using a pump that exhibits various levels of cavitation are run for about 280 hours over a period of 1 month. Several experiments are performed for repeatability and to obtain statistically significant results.

Table III. Cavitation levels staged.

Case Study	Suction Pressure (psi)
Healthy or Baseline	3
Cavitation Level 1	-1
Cavitation Level 2	-2
Cavitation Level 3	-3

2. Pump Impeller Cracks

Impeller damage occurs due to corrosion or when the centrifugal pump is used to transfer fluids that contain solids. Development of impeller cracks is a serious failure mode and it might lead to the loss of material from the impeller blade. This would in turn result in the pump producing reduced work horsepower thereby resulting in loss of flow and loss of efficiency. Hence in this study, cracks in the impeller blades are developed to study the effectiveness of the proposed method in detecting such faults. The results are compared to the vibration-based signal analysis method. Figure 25 shows the different cracks staged on the pump impeller. The numbers marked depict the sequence in which the cracks on the impeller are staged. Figure 26 shows the dimension of each staged crack. Each crack is of approximately the same dimension. Different sets of experiments are staged with each subsequent set consisting of more cracks than the set before. Six different faults are staged on the impeller to test the detection effectiveness of the proposed scheme. Table IV outlines the fault types staged on the pump impeller. Four experiments are conducted for each fault type to demonstrate the repeatability and to obtain statistically significant results. Figure

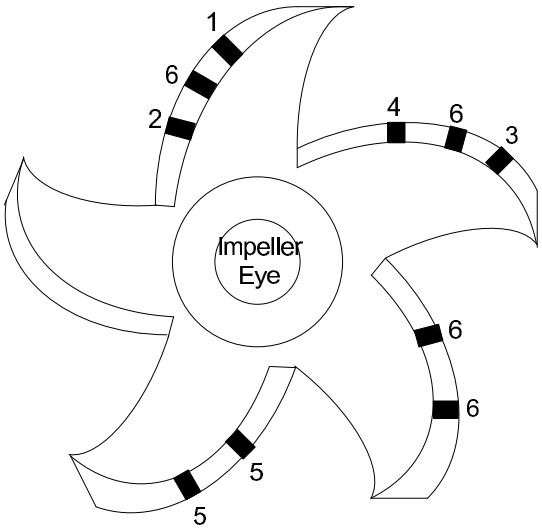

Fig. 25. Schematic of pump impeller with cracks.

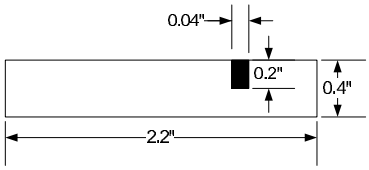

Fig. 26. Dimension of crack staged on the impeller blade.

Table IV. Impeller fault types.

Fault No.	Fault Type
Fault 1	One crack
Fault 2	Two cracks
Fault 3	Three cracks
Fault 4	Four cracks
Fault 5	Six cracks
Fault 6	Ten cracks

27 shows the photograph of the pump impeller with the staged cracks.

Fig. 27. Photograph of the staged impeller cracks.

3. Pump Bearing Damage

Rolling element bearings consist of an inner race, an outer race and set of rollers on a train between the two races. Bearing damage could occur due to various reasons. Some of these include, contamination, improper lubrication, brinelling, etc. Bearing failures can be broadly classified as single-point defects and generalized roughness

faults. In this study, the detection of generalized roughness faults, which is commonly encountered in industrial practice is demonstrated. Recent studies [36, 37, 38] indicate that the electric discharge machining (EDM) process is the most destructive process for damaging a bearing. For EDM to occur, the rollers must be separated from the raceways by a thin film of lubricant. This thin film acts as a dielectric and allows the bearing to act like a capacitor. When the voltage drop across the bearing exceeds the dielectric strength of the bearing, EDM occurs and it damages the bearing. In this study, AC shaft current is passed through the bearing to accelerate the failure process.

Figure 28 and Figure 29 show the schematic and the photograph of the experimental setup with the bearing damage circuit.

The induction motor has two bearings, a 6203 bearing on the fan side and a 6205 bearing on the load side. Both of these bearings are replaced with hybrid ceramic bearings to electrically insulate the bearings from the stator. One of the 6203 bearings in the centrifugal pump is also replaced with a hybrid ceramic bearing. The front bearing of the centrifugal pump is the test bearing under consideration. AC current is injected into the motor shaft through an external single phase AC power source. Since the motor side is electrically insulated, current flows through the test bearing on the centrifugal pump and returns through the pump casing. Two power resistors are placed to limit the shaft current. Using the EDM technique, the amount of time it takes to damage a bearing depends on two factors. One is the magnitude of the shaft current and the other is the amount of grease present in the bearing. In [36], it is stated that with 12 A shaft current, it takes about 2 to 3 weeks to damage a new bearing. In this study, AC current of magnitude of about 6A is injected through the test bearing. To reduce the time to failure of the bearing, some grease is removed from the test bearing. To accomplish this, the bearing is immersed in a degreasing

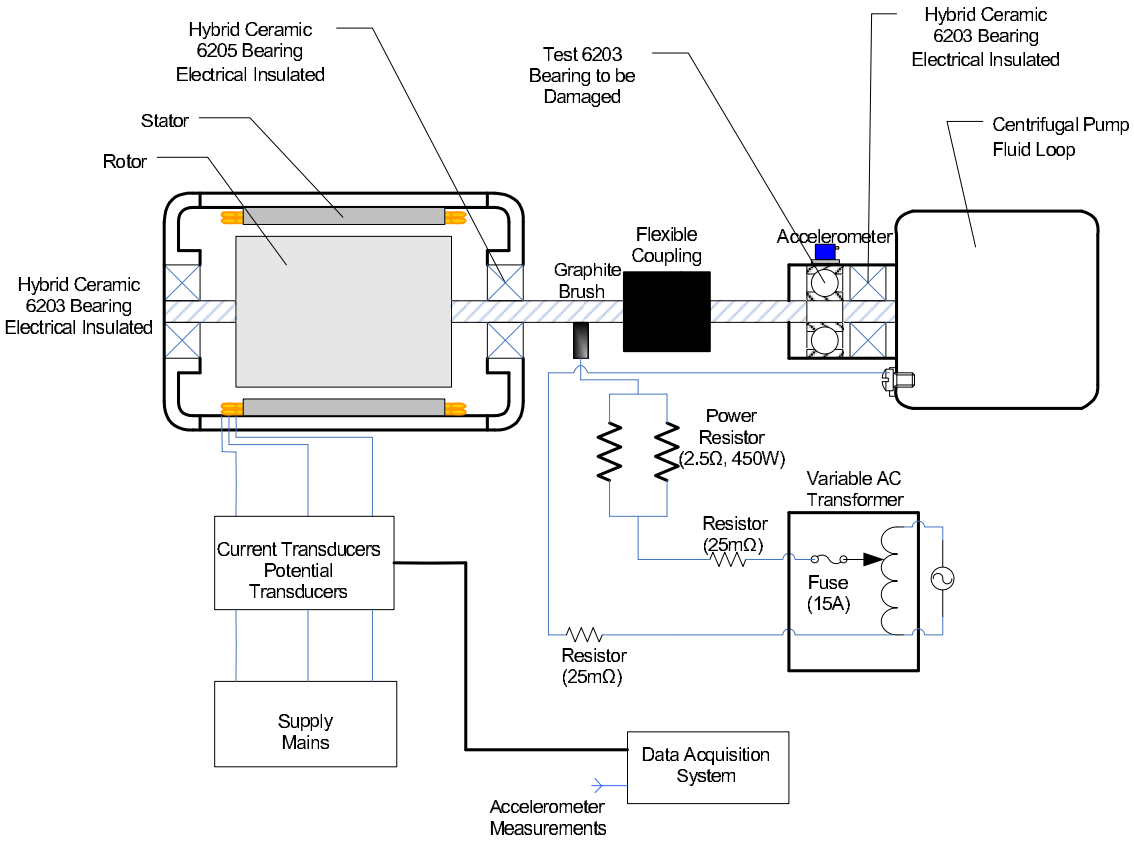

Fig. 28. Bearing damage circuit schematic.

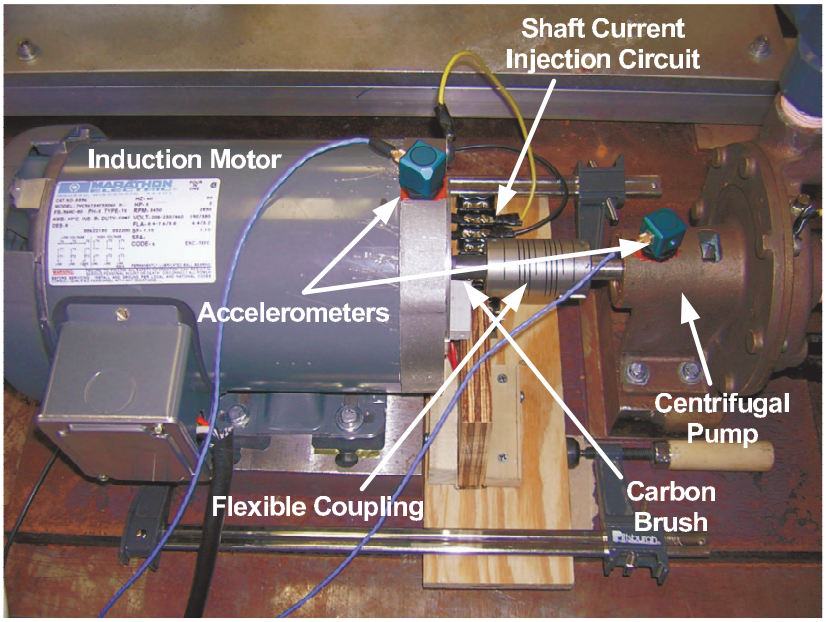

Fig. 29. Photograph of the experimental setup with the bearing damage circuit.

solution to remove all the grease. The bearing is then filled with a known amount of grease. The volume of the bearing is obtained and then a percentage of the volume is chosen as the amount of the grease to be filled. In this study, the bearing is repacked with an approximate fill of 3% to 5% by volume. The factory standard is about 20% to 40% by volume [35]. In this study, with the injected current fixed at 6 A and the bearing grease fill fixed at about 3% to 5% by volume, the failure time for the bearing is reduced to about 24 to 36 hours. Four sets of experiments are conducted to demonstrate the repeatability and to obtain statistically significant results.

D. Fault Detection Results

1. Pump Cavitation Results

Figure 30 shows the vibration level change for the first set of experiments. The pump does not exhibit any cavitation during the first 100 hours. The first level of cavitation is staged around the 101^{st} hour, the second level of cavitation around the 160^{th} hour and the third cavitation level at around the 220^{th} hour.

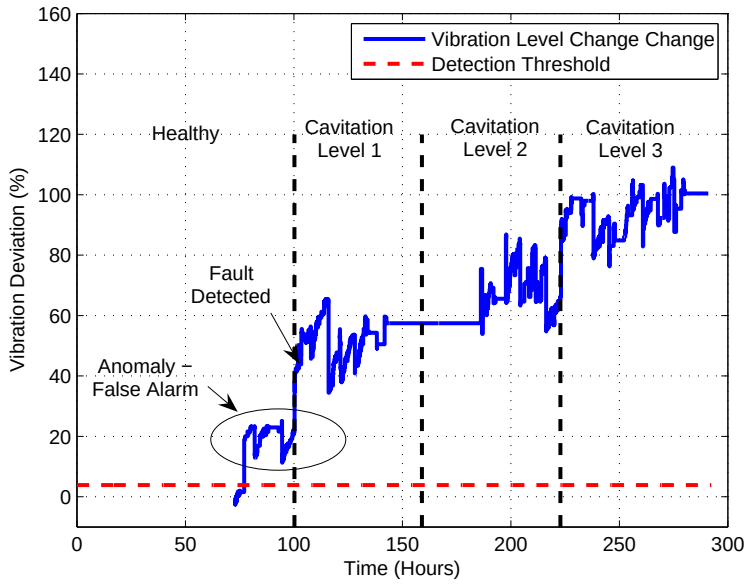

Fig. 30. Experiment 1 of pump cavitation fault; Vibration level change.

Note that, the vibration level suddenly increases even before the fault is staged, thereby producing a false alarm. If we account for this false alarm and re-compute the vibration detection threshold, then the vibration-based signal analysis detects the presence of cavitation at around the 101^{st} hour, immediately after its introduction. This false alarm phenomenon is not observed in the proposed fault detection method.

Figure 31 shows the proposed FDIC for the same case for all the induced cavitation fault levels. Cavitation can be detected at around the 116^{th} hour using the proposed method.

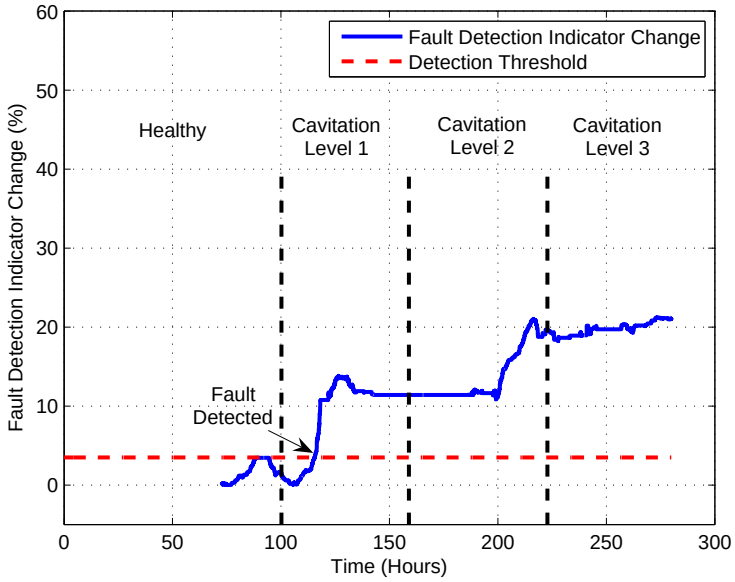

Fig. 31. Experiment 1 of pump cavitation fault; Proposed FDIC.

Figure 32 shows the vibration level change for the second set of experiments and Figure 33 shows the equivalent FDIC for the same case for all the cavitation fault levels. The fault can be detected at around the 102^{nd} hour using the vibration indicator and around the 105^{th} hour using the proposed fault detection method. In both sets of experiments, the proposed technique detects the presence of cavitation during the very initial stages, although it slightly lags the vibration-based signal analysis.

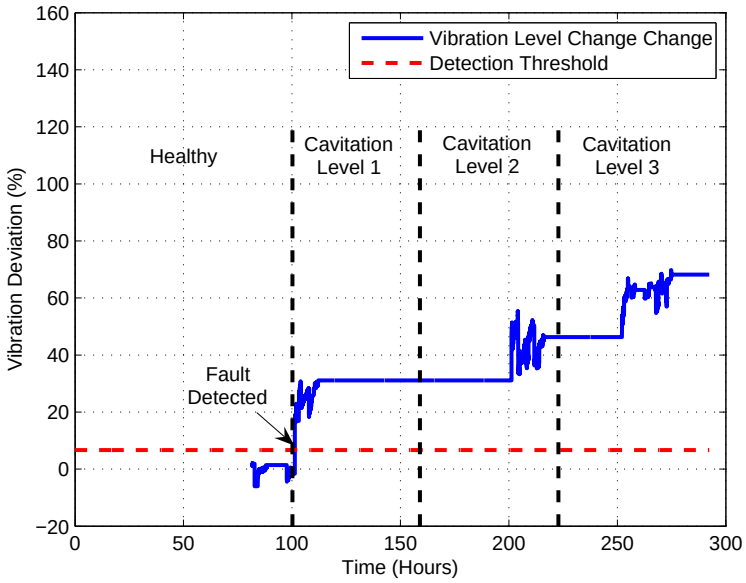

Fig. 32. Experiment 2 of pump cavitation fault; Vibration level change.

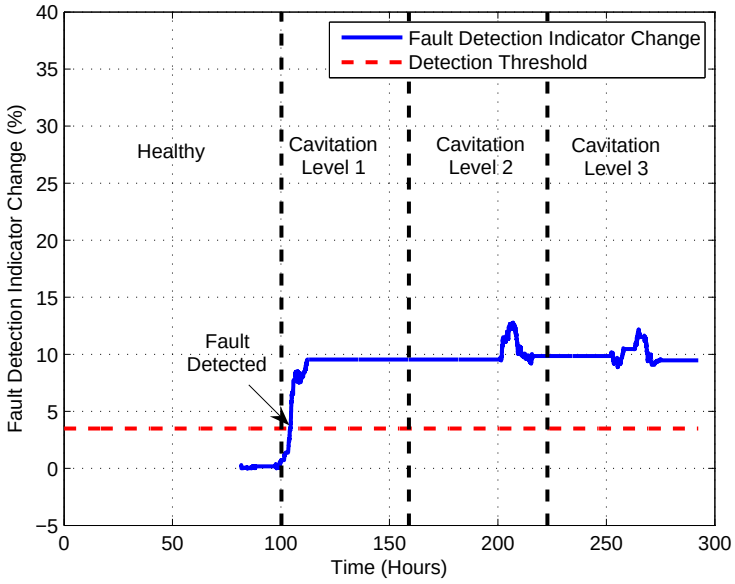

Fig. 33. Experiment 2 of pump cavitation fault; Proposed FDIC.

Table V. Pump impeller cracks; time instant of staged fault.

Fault Type	Fault 1	Fault 2	Fault 3	Fault 4	Fault 5	Fault 6
Fault Staging Time (Hour)	101	198	258	317	368	422

2. Pump Impeller Cracks Results

Table V shows the time instant at which each impeller crack fault type is staged. As more cracks are staged on the impeller blades, some amount of imbalance is created in the impeller, which in turn induces changes in the torque transmitted from the motor. As the number of cracks increases, this imbalance increases and the severity of the fault increases.

Figure 34 shows the vibration level change for all of the impeller fault types for the first set of experiments. Note that the vibration signal increases beyond the detection threshold even before the fault is staged. After some time, the vibration level drops below the threshold. None of the first 5 faults can be detected using the vibration indicator. Only Fault 6 is detected at around the 420^{th} hour. Figure 35 shows the proposed FDIC for all impeller fault types for the same case. The proposed method detects the presence of the fault at around the 137^{th} hour. Note that there is a slight drop in the FDIC for fault 5. This could be attributed to the location of the 5^{th} and the 6^{th} cracks staged. The 5^{th} and the 6^{th} staged cracks on the impeller blade are diametrically opposite to the 1^{st} and the 2^{nd} staged cracks. Hence this improves the balance of the impeller compared to the first four cracks. Eventhough the balance is not perfect, it is sufficient to cause the cancelation of the two sequences of staged

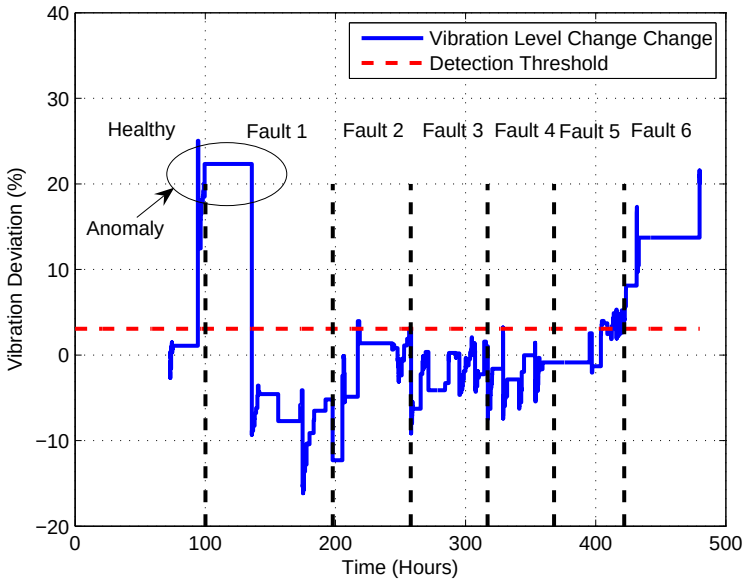

Fig. 34. Experiment 1 of pump impeller fault; Vibration level change.

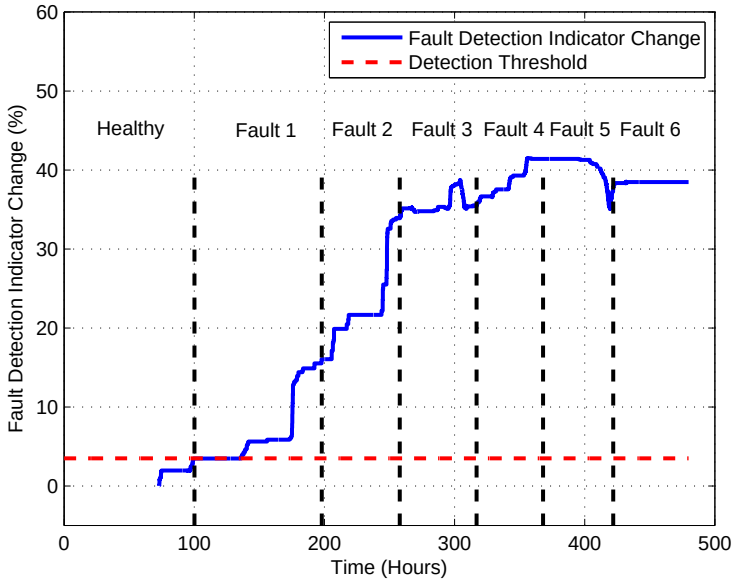

Fig. 35. Experiment 1 of pump impeller fault; Proposed FDIC.

faults.

Figure 36 and Figure 37 shows the vibration level change and the proposed FDIC for all of the impeller fault types for the second set of experiments. Even in this experiment, the vibration indicator does not detect the first 5 faults and detects fault 6 at around the 422^{nd} hour. While the proposed method detects the impeller fault at around the 140^{th} hour.

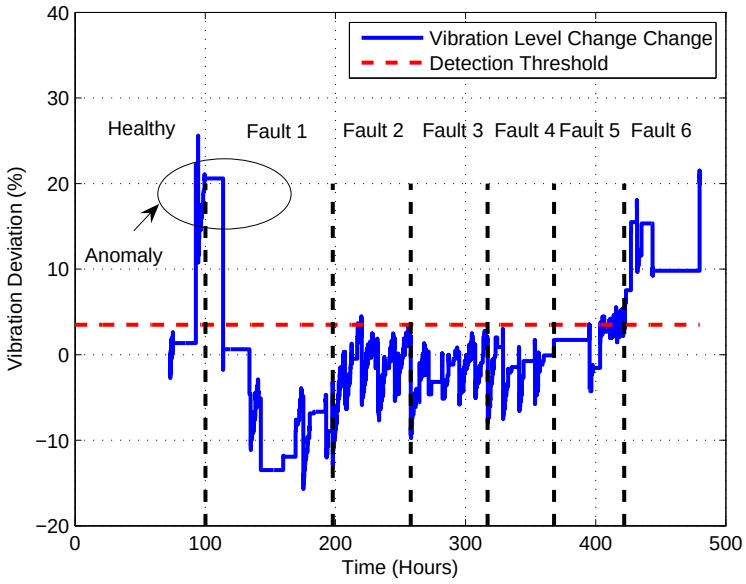

Fig. 36. Experiment 2 of pump impeller fault; Vibration level change.

3. Pump Damaged Bearing Results

Figure 38 shows one of the bearings damaged using the EDM process. Surface roughness of the outer race and inner race can be seen and no significant pits are seen on the surfaces. Figure 39 shows the vibration level change and the proposed FDIC for the first bearing damage experiment. In this experiment, the AC current is injected

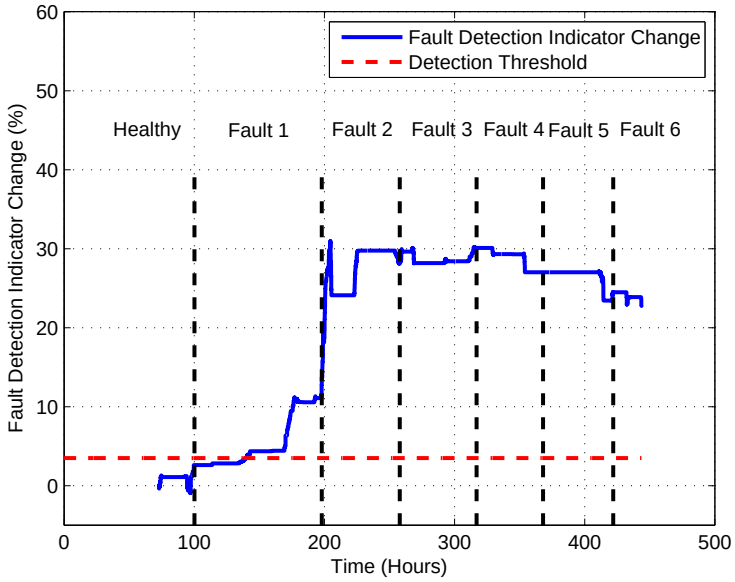

Fig. 37. Experiment 2 of pump impeller fault; Proposed FDIC.

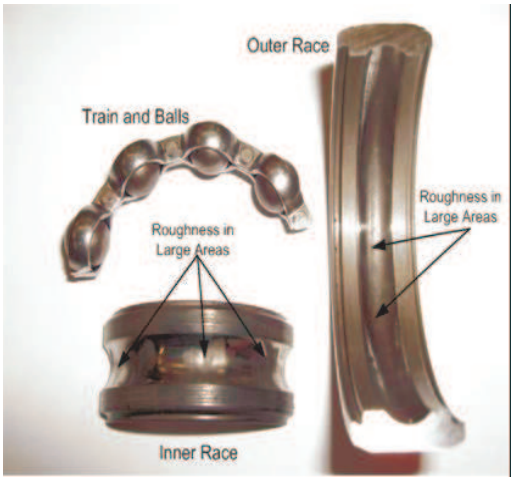

Fig. 38. A bearing damaged using the EDM process.

at around the 11^{th} hour. The fault is detected around the 14^{th} hour using the proposed detection method and around the 16^{th} hour using the vibration indicator. The vibration level change exceeds the detection threshold during certain time instants, but immediately falls below the threshold thereafter. This cannot be considered as a false alarm since the vibration level change does not remain above the threshold sufficiently long enough to call it a false alarm.

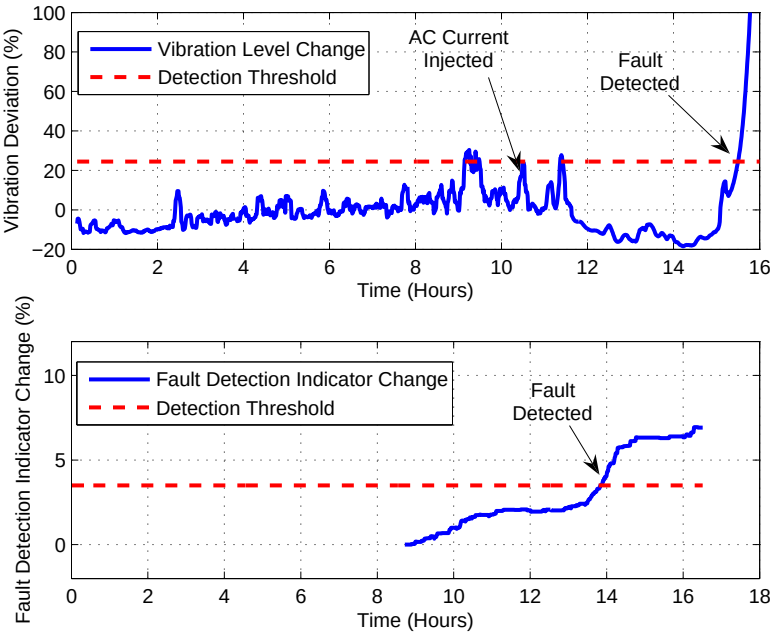

Fig. 39. Experiment 1 of pump bearing fault; Vibration level change in the early stage (top) ; Proposed FDIC (bottom).

Figure 40 shows the vibration level change and the proposed FDIC for the second bearing damage experiment. In this experiment, the AC current is injected at around the 11^{th} hour. The fault is detected at around the 14^{th} hour using the proposed detection method and at around the 13^{th} hour using the vibration indicator.

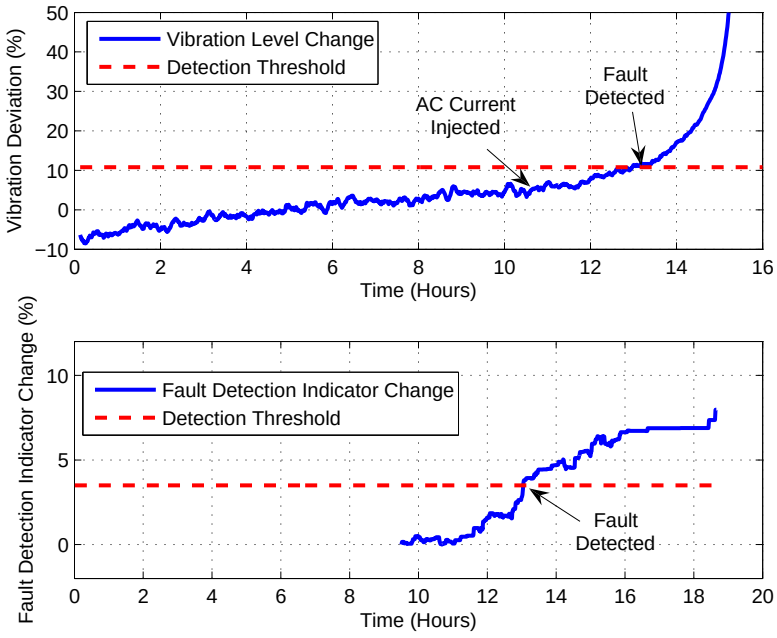

Fig. 40. Experiment 2 of pump bearing fault; Vibration level change in the early stage (top) ; Proposed FDIC (bottom).

4. Summary of All Fault Detection Case Studies

All case studies used to demonstrate the detection effectiveness of the proposed fault detection method are summarized in Table VI. For the cavitation and bad impeller case studies, the fault initiation time is the time instant when the first fault level is staged. Whereas for the damaged bearing cases, the fault initiation time refers to the time instant when the AC current is injected through the bearing. For the cavitation case studies, the average detection time is around hour 111 using the proposed method and around hour 102 using the vibration indicator. For the cracked impeller cases, the average detection times are around hour 135 and hour 422 using the proposed method and vibration indicator, respectively. Similarly, for the damaged bearing cases, the detection times are around hour 13 and hour 16 using the proposed method and vibration indicator, respectively.

In the cracked impeller and the damaged bearing case studies, the vibration indicator lags the proposed method while in the case of cavitation, the vibration indicator detects the fault earlier. However, the vibration detection threshold used in the industry is much higher than the ones used in this study. The usual practice in the industry is to use a vibration detection threshold of about 200%. The reason for this is the sensitivity of vibration analysis in generating frequent false alarms. If this detection threshold is used, then the vibration-based signal analysis will not detect any of the faults staged. However, the proposed method is able to detect the incipient faults that are staged well in advance without running the risk of generating false alarms.

Table VI. Summary of fault detection case studies.

Staged Fault	Case Study	Fault Initiation Time (Hr)	Proposed FDI Detection Time (Hr)	Vibration Detection Time (Hr)
Cavitation	1	101	116	101
	2	101	105	102
Impeller Cracks	1	101	137	420
	2	101	140	422
	3	101	135	420
	4	101	126	424
Bearing Damage	1	11	14	16
	2	11	14	13
	3	11	15	21
	4	11	12	13

E. Fault Isolation Results

Once the effectiveness of the proposed fault detection method is established, the next step is to validate the performance of the fault isolation method. The proposed method presented in the previous section detects the presence of a fault in the system, but it does not give any information as to which component in the system has a fault. That is, it does not distinguish between a fault in the motor and a fault in the pump. Whether there is a motor or a pump fault, the proposed FDIC goes above the detection threshold thereby raising an alarm. The proposed fault isolation indicator distinguishes between motor related faults and pump related faults. Note that the fault isolation is performed only when the proposed detection method detects the presence of fault within the system. In this study, bearing faults are used to evaluate the performance of the proposed fault isolation method. Four different cases are studied to validate the fault isolation effectiveness as follows:

1. *Case 1 - "Healthy":* In this case, there is no fault in the system. Both the motor and the pump are "healthy".

2. *Case 2 - Fault in Motor:* The motor bearing is damaged, whereas the pump is "healthy".

3. *Case 3 - Fault in Pump:* The pump bearing is damaged, while the motor is "healthy".

4. *Case 4 - Fault in Motor and Pump:* Both the motor and pump bearings are damaged.

1. Case 1 - "Healthy" System

"Healthy" experiments are divided into two groups. The first group of experiments are conducted to study the effects of loading changes on the fault isolation indicator (FII). Four separate experiments are performed at 20%, 36%, 38% and 40% loading levels. The 20% load level is considered as the baseline and the percentage change in the FII with respect to this baseline is computed. Similarly, the current RMS percentage change and the voltage RMS percentage change are computed. Figure 41 and Figure 42 shows the percentage change in the voltage RMS and the current RMS, respectively.

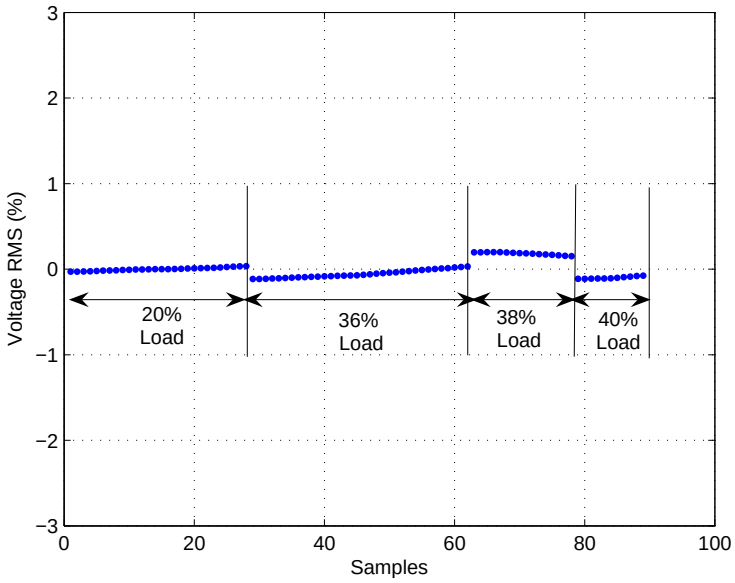

Fig. 41. Voltage RMS at different loading levels.

Figure 43 shows the proposed fault isolation indicator change (FIIC) with respect to the 20% load level baseline condition. As the current RMS increases, the proposed FII also increases thereby showing a strong linear relationship as shown in Figure 44.

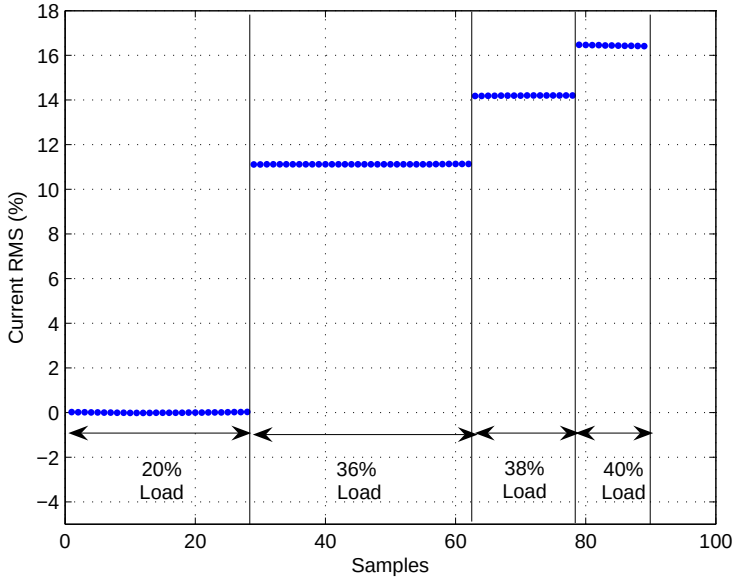

Fig. 42. Current RMS at different loading levels.

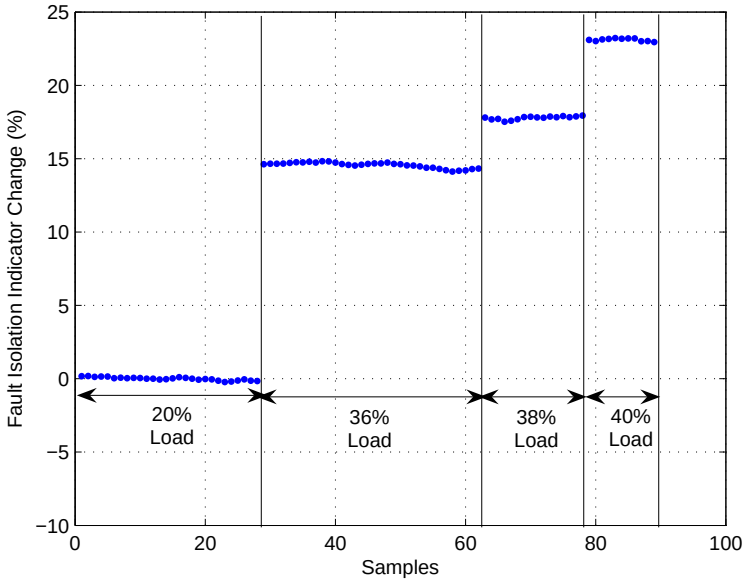

Fig. 43. Proposed FIIC at different loading levels.

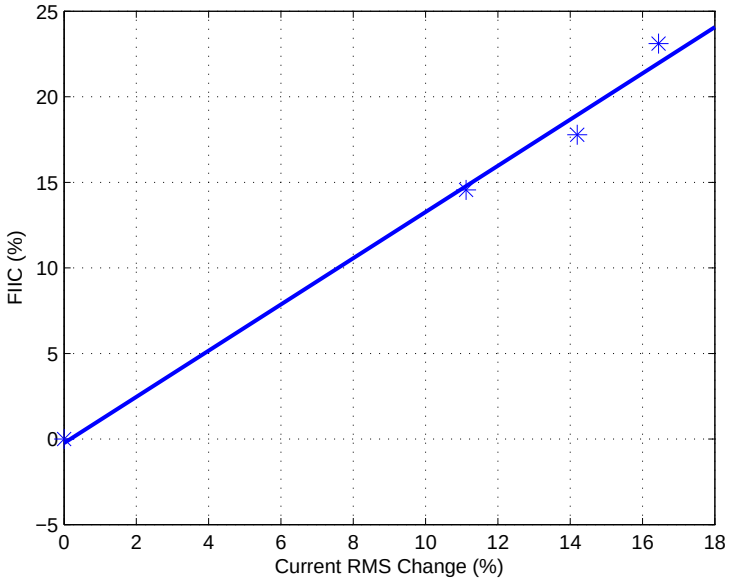

Fig. 44. Proposed FIIC versus current RMS change.

The second group of experiments are conducted with the system in "healthy" condition in order to explore the generated rates of false alarms. Over 15 case studies are conducted to ensure repeatability and to obtain statistically significant results. Figure 45 shows the proposed FIIC with respect to a baseline for three such experiments. Figure 46, Figure 47 and Figure 48 show the details of Figure 45 for each of the individual data sets. The deviations of the proposed FII with respect to the mean for each of the three data sets are very small. A detection threshold is not set as the "healthy" baseline may vary depending on the motor load. Hence adaptive detection thresholds are used to check whether the proposed FII exceeds these threshold values. A multiple of the standard deviation of the "healthy" baseline is considered as the detection threshold for the proposed FII.

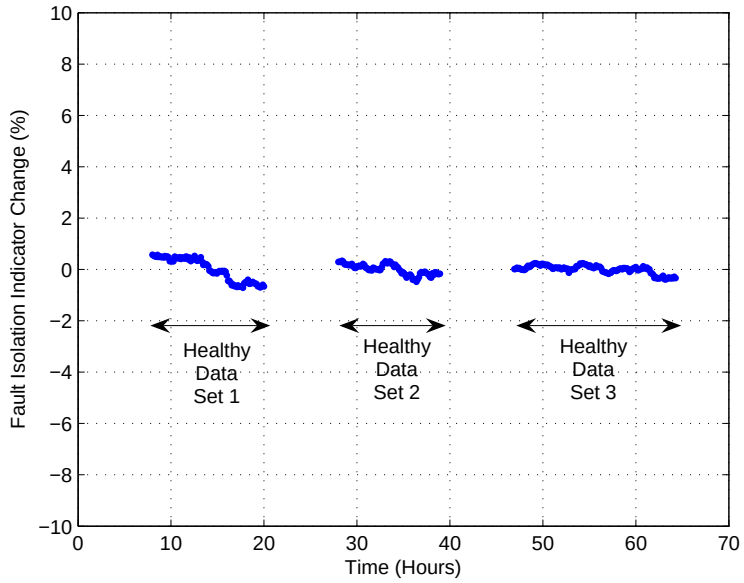

Fig. 45. Proposed FIIC for three "healthy" data sets.

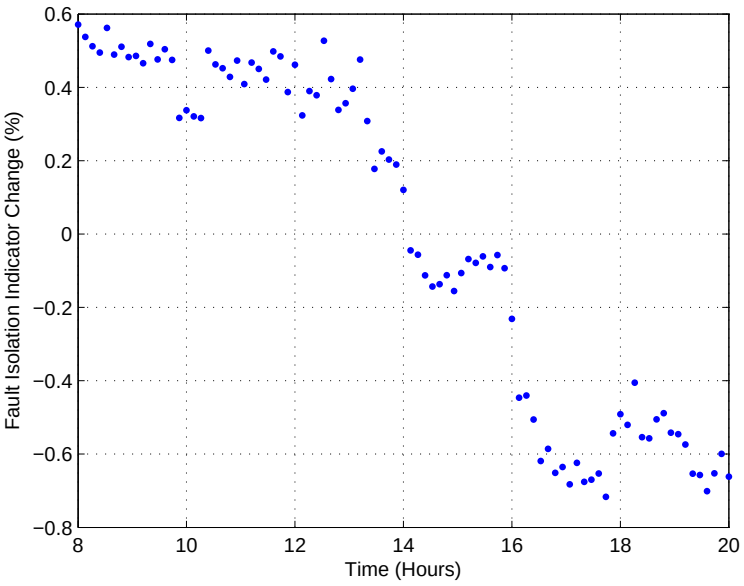

Fig. 46. Proposed FIIC for data set 1.

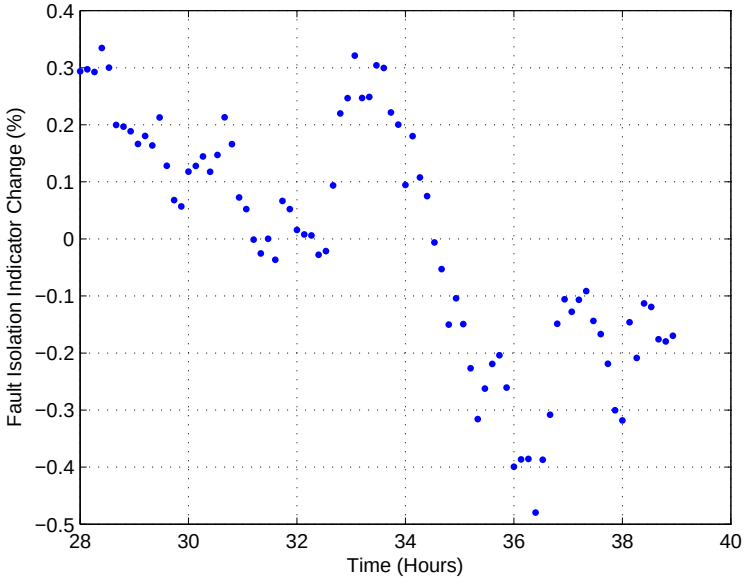

Fig. 47. Proposed FIIC for data set 2.

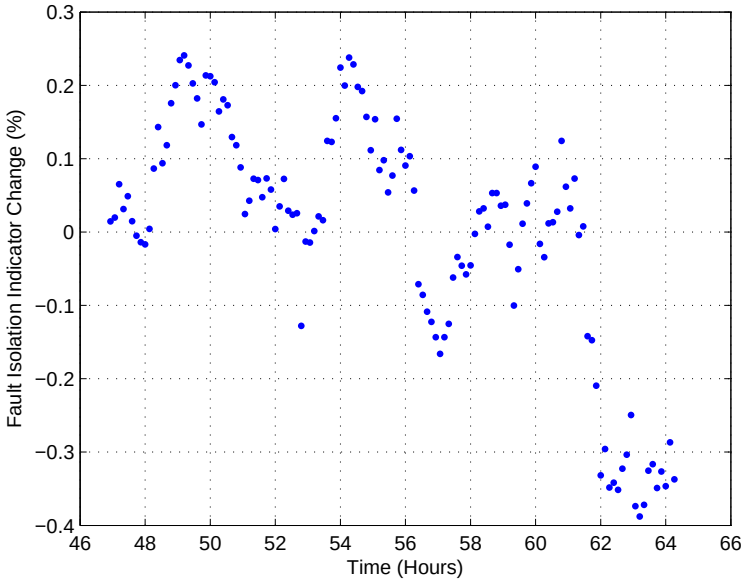

Fig. 48. Proposed FIIC for data set 3.

2. Case 2 - Fault in the Motor

This case study deals with damaging a motor bearing, while the pump bearing is "healthy". The load side 6205 bearing is damaged using the EDM process. AC current of about 8 A to 12 A is passed through the test bearing to accelerate the failure process. The fan side 6203 bearing is replaced with a hybrid ceramic bearing to electrically insulate it from the stator and to force the injected current through the test bearing. Three different experiments are staged at different loading levels, one at 0%, one at 20% and one at 40% of the rated load level. As the condition of the bearing deteriorates, the output torque produced by the motor reduces, which in turn results in the pump producing less work output. Since there is no feedback from the fluid loop (adjusting the flow rate), the motor output power reduces as the bearing degrades. This leads to a decrease in the motor current.

The top portion of Figure 49 shows the proposed FDIC for the 0% load condition. The AC current is injected through the test bearing at around the 5^{th}hour. The proposed method detects the presence of a fault in the motor-pump system at around the 12^{th} hour. However, the proposed FDIC alone is not sufficient to isolate the fault. The fault could be either in the motor or the pump. Hence, further investigation is required to isolate the fault. The developed fault isolation model is a localized model of the induction motor and hence, the proposed FII is only sensitive to faults in the motor, while being insensitive to faults in the pump. Therefore, if the fault in the system is present in the motor, then the proposed FII must increase and be larger than that obtained during the baseline "healthy" operation. Based on the middle and the bottom portion of Figure 49, it can be concluded that after the fault initiation, since the proposed FII increases inspite of the drop in the current RMS, the fault is in fact in the motor and not in the pump.

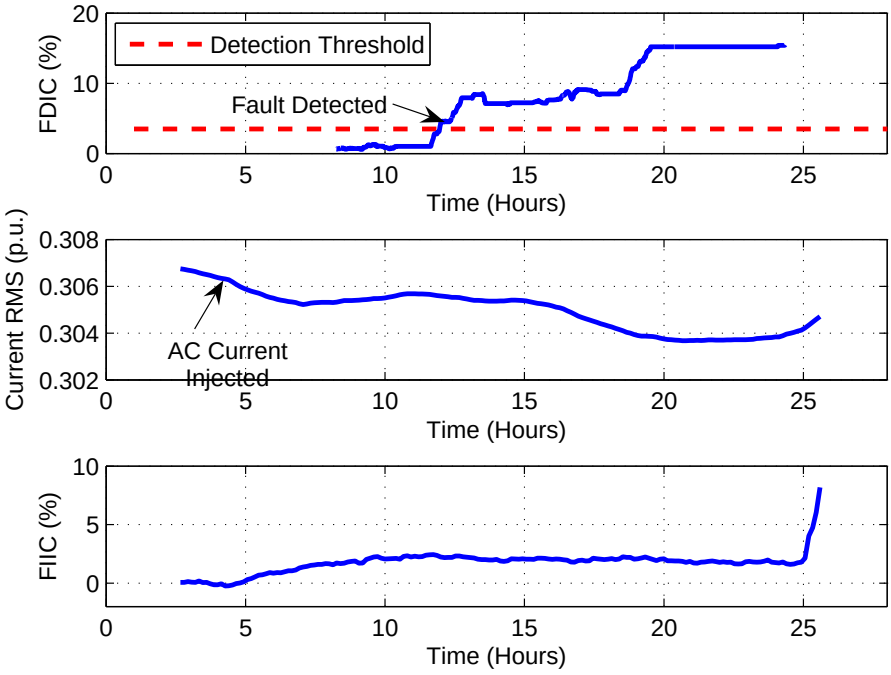

Fig. 49. Motor bearing fault - 0% load level; Proposed FDIC (top); Current RMS change (middle); Proposed FIIC (bottom).

Figure 50 and Figure 51 show the proposed FDIC, current RMS change and the proposed FIIC for the 20% and 40% load conditions, respectively. The AC current

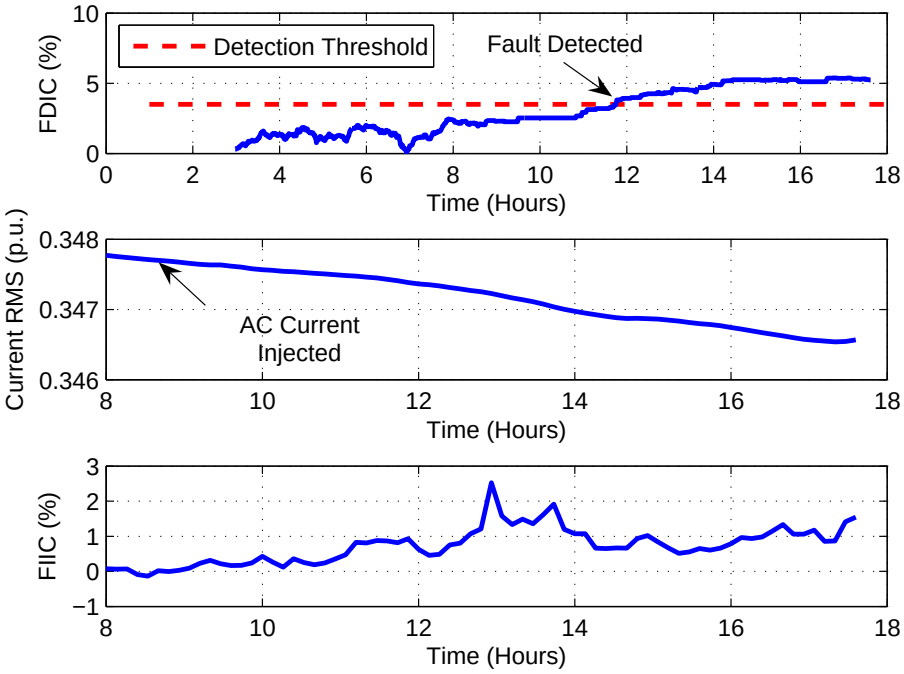

Fig. 50. Motor bearing fault - 20% load level; Proposed FDIC (top); Current RMS change (middle); Proposed FIIC (bottom).

for both the experiments is injected through the test bearing at around the 9^{th}hour. In both these experiments the proposed method detects the presence of a fault within the system at around the 12^{th} hour and 13^{th} hour, respectively. It can be noted that, since the proposed FII is sensitive to faults in the motor, the proposed FIIC increases beyond the baseline "healthy" value eventhough the current RMS decreases after the initiation of the fault, thereby indicating that the fault is in the motor.

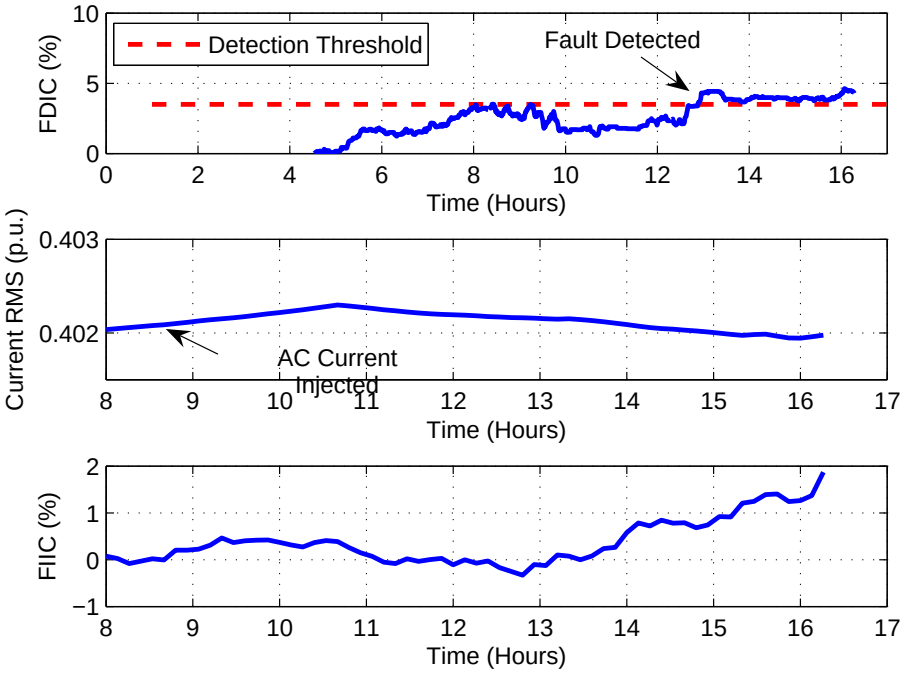

Fig. 51. Motor bearing fault - 40% load level; Proposed FDIC (top); Current RMS change (middle); Proposed FIIC (bottom).

3. Case 3 - Fault in the Pump

In this case study, the pump bearing is damaged using the EDM process described in the previous chapter. As the pump bearing is damaged the work output of the pump reduces which in turn results in the decrease of the input mechanical power. This decrease in the input power leads to a decrease in the motor current. Three separate experiments are performed to ensure repeatability and to obtain statistically significant results. AC current of about 6 A is passed through the test bearing to accelerate its failure. The AC current for all the experiments is injected through the test bearing at around the 11^{th}hour.

Figure 52 shows the proposed FDIC, current RMS change and the proposed FIIC for the first pump bearing damage experiment. The top portion of the figure shows that the proposed fault detection method detects the presence of the fault within the system at around the 14^{th} hour. As explained in the previous subsection, this information alone is not sufficient to isolate the fault and hence the fault isolation method has to be employed to distinguish between motor and pump faults. Since the proposed FII is insensitive to faults in the pump, the proposed FIIC should not increase and exceed the value obtained during the baseline "healthy" operation of the motor-pump system. Based on the middle and the bottom portion of Figure 52, it can be concluded that since the proposed FII decreases with the decreasing current RMS after the initiation of the fault, the fault is in fact in the pump and not in the motor.

Figure 53 and Figure 54 show the proposed FDIC, current RMS change and the proposed FIIC for the second and the third pump bearing damage experiments, respectively. In both these experiments the proposed method detects the presence of a fault within the system at around the 14^{th} hour and 15^{th} hour, respectively.

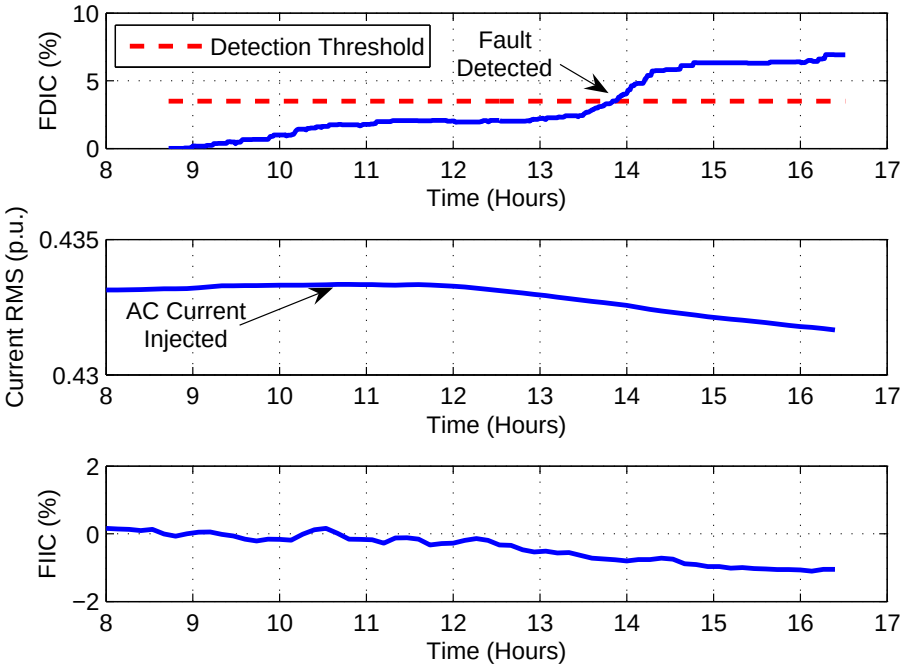

Fig. 52. Experiment 1 of pump bearing fault; Proposed FDIC (top); Current RMS change (middle); Proposed FIIC (bottom).

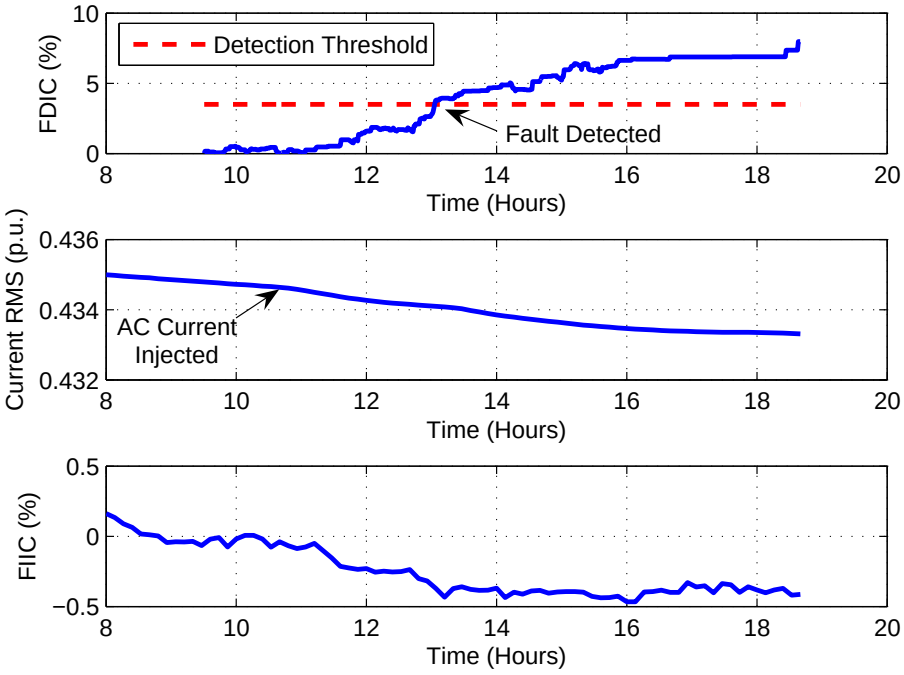

Fig. 53. Experiment 2 of pump bearing fault; Proposed FDIC (top); Current RMS change (middle); Proposed FIIC (bottom).

It can be noted that, since the proposed FII is insensitive to faults in the pump, the proposed FIIC decreases with the current RMS after the initiation of the fault, thereby indicating that the fault is in the pump and not in the motor.

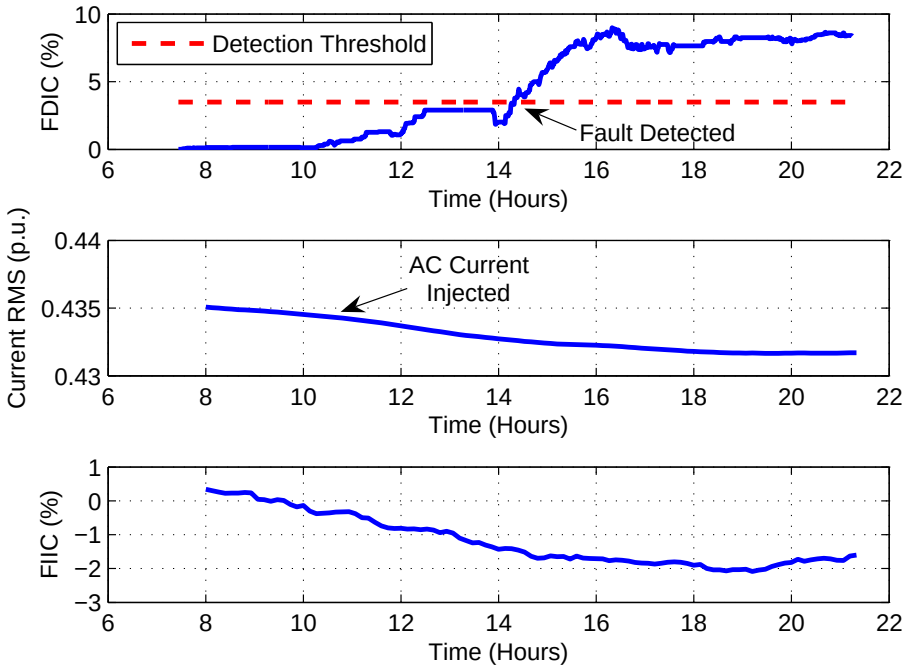

Fig. 54. Experiment 3 of pump bearing fault; Proposed FDIC (top); Current RMS change (middle); Proposed FIIC (bottom).

4. Case 4 - Fault in the Motor and the Pump

In this case study, the motor load side bearing and the pump bearing are damaged simultaneously. Due to the different sizes of the bearing (6203 bearing in the pump and 6205 bearing in the motor), the failure rate of the bearings could not be controlled accurately and hence one bearing damaged more than the other. Moreover, due to the smaller size, the pump bearing fails earlier than the motor bearing. Three different

experiments are conducted to obtain statistically significant results, out of which only two are presented here. Figure 55 shows the vibration level change for one of the experiments. The AC current is injected at around the 11^{th} hour. The pump bearing vibration crosses the detection threshold at around the 13^{th} hour, whereas the motor bearing vibration crosses the detection threshold at around the 15^{th} hour.

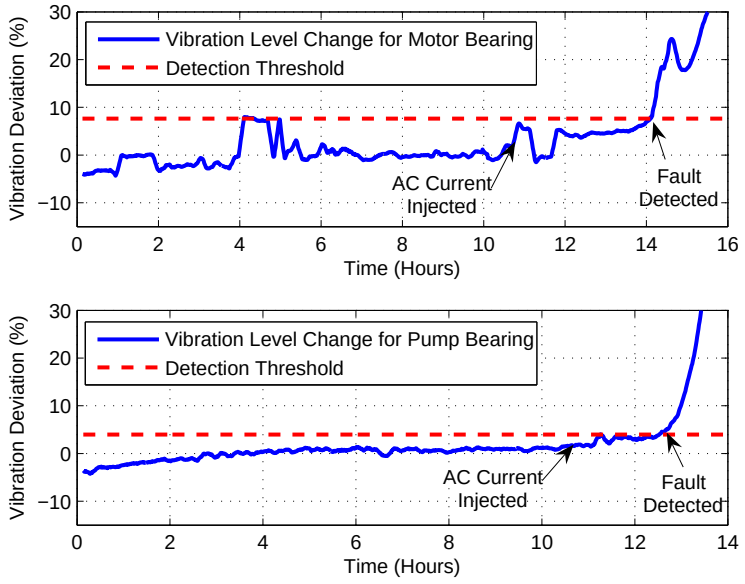

Fig. 55. Experiment 1 of motor and pump bearing fault; Vibration level change for motor bearing (top); Vibration level change for pump bearing (bottom).

Figure 56 shows the proposed FDIC, current RMS change and the proposed FIIC for the first set of experiments. The proposed fault detection method detects the bearing fault at around the 13^{th} hour as shown in the top portion of the figure. After the initiation of the fault, since the pump bearing starts to fail first (as can be seen from the vibration plots), the proposed FII being insensitive to the pump fault starts to decrease as the load on the motor decreases. After a while, the motor bearing starts to fail. At this time, the proposed FII being sensitive to motor faults

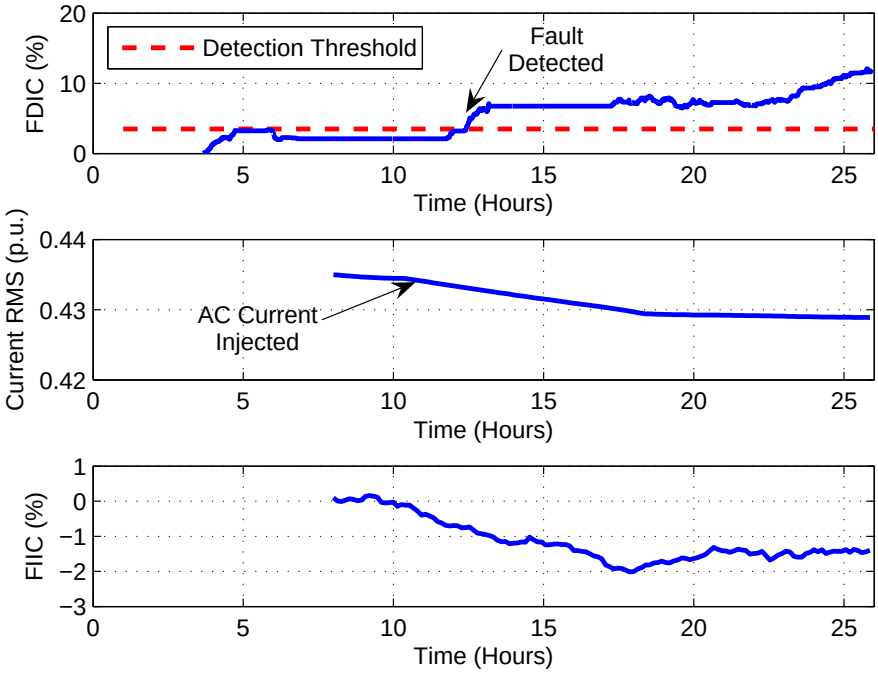

Fig. 56. Experiment 1 of motor and pump bearing fault; Proposed FDIC (top); Current RMS change (middle); Proposed FIIC (bottom).

starts to increase. But the pump bearing continues to degrade further. Hence due to the cancelation effect, the FIIC starts to flatten out thereby indicating the existence of the fault in both the motor and the pump.

Figure 57 shows the vibration level change for the second set of experiments. The AC current is injected at around the 11^{th} hour. The pump bearing vibration

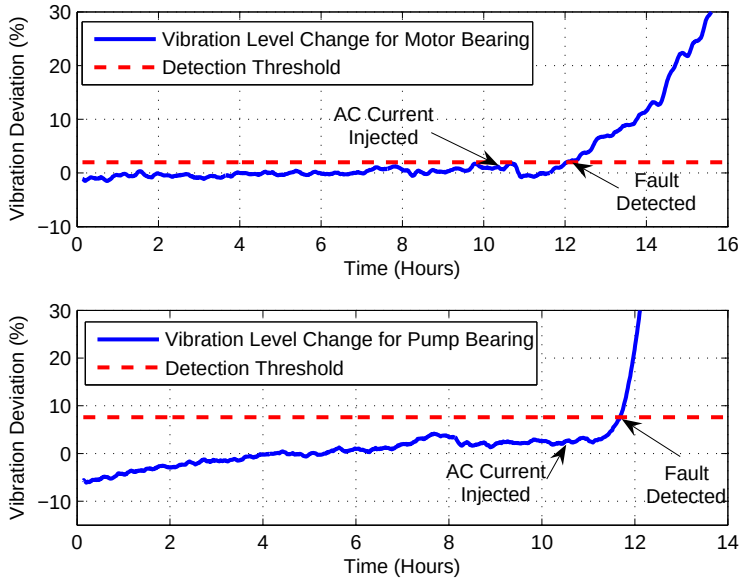

Fig. 57. Experiment 2 of motor and pump bearing fault; Vibration level change for motor bearing (top); Vibration level change for pump bearing (bottom).

crosses the detection threshold at around the 12^{th} hour, whereas the motor bearing vibration crosses the detection threshold at around the 13^{th} hour. Even in this case, the pump bearing starts to fail earlier than the motor bearing. Figure 58 shows the proposed FDIC, current RMS change and the proposed FIIC for the second motor and pump bearing damage experiment. Using the proposed detection method, the bearing fault is detected at around the 13^{th} hour. Since the pump bearing fails first, the proposed FIIC being insensitive starts to decrease and when the motor bearing

also starts to fail, the proposed FIIC stabilizes thereby indicating that both the motor and the pump is faulty.

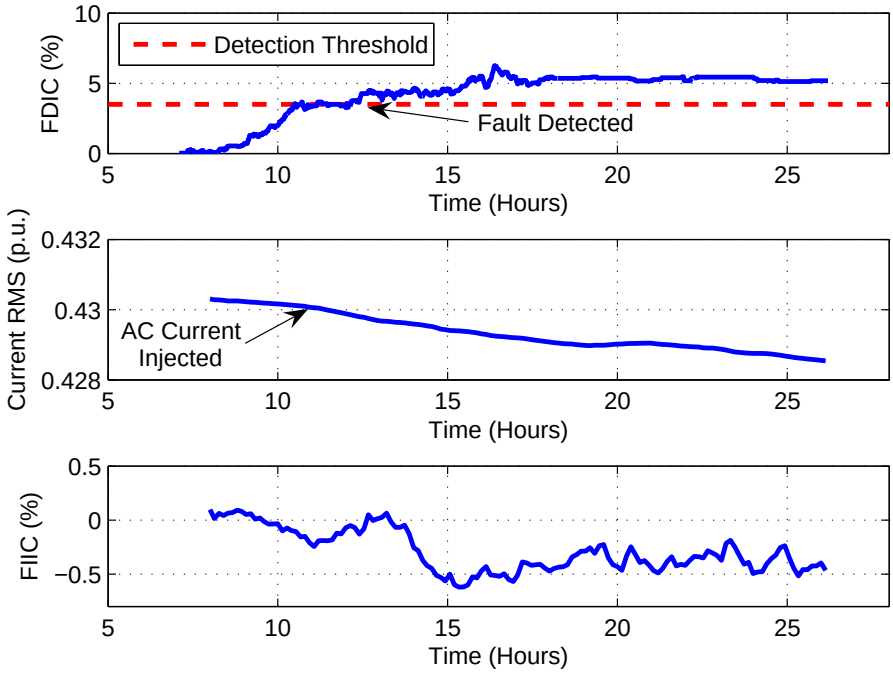

Fig. 58. Experiment 2 of motor and pump bearing fault; Proposed FDIC (top); Current RMS change (middle); Proposed FIIC (bottom).

F. Summary of All Fault Isolation Case Studies

Four cases are studied to evaluate the performance of the fault isolation algorithm. Based on the results presented in the previous subsections, the following observations can be made:

- If the system is "healthy", i.e., both the motor and the pump are "healthy", then the proposed FDIC is below the detection threshold. There is no requirement

to investigate the isolation problem.

- If a fault exists in the motor, then the proposed FDIC exceeds the detection threshold. The proposed FII being sensitive to motor faults increases beyond the value obtained during the baseline "healthy" operation. The motor current decreases as the load reduces due to the initiation of the fault. Hence there is a negative correlation between the current RMS and the proposed FII.

- If a fault exists in the pump, then the proposed FDIC exceeds the detection threshold. However, the proposed FII is insensitive to pump faults and hence decreases with the decreasing motor current as even in this case, the motor load reduces due to the initiation of the fault. Hence there is a strong positive correlation between the motor current and the proposed FII.

- If a fault exists in both the motor and the pump, then the proposed FDIC exceeds the detection threshold similar to the other cases. Considering that the fault initiates initially in the pump and then in the motor, the proposed FII starts to decrease first due to the pump fault and then stabilizes when a motor component also starts to fail. Hence the correlation between the motor current and the proposed FII is not strong.

The fault isolation results are summarized in Table VII.

G. Impact of Motor and Centrifugal Pump Faults on Motor and System Efficiency

As the components within a system begin to deteriorate, the system efficiency starts to decrease. Hence early fault detection systems have found considerable applications in detecting incipient faults and alerting plant personnel to schedule the required maintenance. In this study, the effects of bearing degradation on motor and overall

Table VII. Summary of fault isolation case studies.

Proposed FDI	Proposed FII	Correlation (FII vs Current RMS)	Diagnosis
Below Threshold	N/A	N/A	"Healthy"
Above Threshold	Increases	Negative	Motor Fault
Above Threshold	Decreases	Positive	Pump Fault
Above Threshold	Decreases or Increases	Weak Positive or Negative	Motor and Pump Fault

system efficiency are studied. Two sets of experiments are conducted, one with only the motor bearing damaged and the other with both motor and pump bearing damaged. The data from the experiment with only the motor bearing damaged is used to compute the change in motor efficiency, while the data from the experiment with both the motor and the pump bearings damaged is used to compute the change in the overall system efficiency.

Efficiency is defined as the ratio of the output power to the input power. Efficiency of the motor is given as:

$$\text{Motor Efficiency} \quad = \quad \frac{\text{Mechanical Output Power}}{\text{Electrical Input Power}}. \tag{5.1}$$

The efficiency of a centrifugal pump is given as:

$$\text{Pump Efficiency} \quad = \quad \frac{\text{Work Horsepower}}{\text{Brake Horsepower}}, \tag{5.2}$$

where the work horsepower is given as

$$\text{Work Horsepower} = \frac{Q \times H \times sp.gr}{3960}, \tag{5.3}$$

Table VIII. Impact of bearing degradation on motor efficiency.

Motor Condition	Electrical Input Power (hp)	Mechanical Output Power (hp)	Motor Vibration Level (V)	Motor Efficiency (%)
"Healthy"	1.15	0.91	0.09	79.1
Faulty	1.14	0.86	1.11	75.4

where, Q is the flow in gpm, H is the total differential head in ft and $sp.gr$ is the specific gravity of the fluid being pumped.

The overall system efficiency is then given as:

$$\text{System Efficiency} = \frac{\text{Work Horsepower}}{\text{Electrical Input Power}}. \tag{5.4}$$

In this study, water is the fluid used in the pump. Hence the $sp.gr$ is equal to 1. The motor electrical input power and the mechanical output power are calculated based on IEEE standard 112 [39], outlined in Appendix A. Table VIII shows the impact of motor bearing degradation on motor efficiency. The motor bearing vibration increases from 0.09V to 1.11V, which is an increase of about 1100%. The decrease in the motor efficiency due to bearing degradation is about 3.7%. Table IX shows the impact of motor and pump bearing damage on the overall system efficiency. The change in the motor bearing vibration is about 333% and the change in the pump bearing vibration is about 125%. The change in the overall system efficiency is about 3.3%.

One would expect that, if both the pump bearing and the motor bearing are damaged, the drop in the efficiency would be larger than, if only the motor bearing is damaged. However, the efficiency drop is also related to the severity of the bearing

Table IX. Impact of bearing degradation on overall system efficiency.

Motor and Pump Condition	Motor Electrical Input Power (hp)	Pump Output Power (hp)	Motor Vibration Level (V)	Pump Vibration Level (V)	System Efficiency (%)
"Healthy"	1.27	0.77	0.03	0.08	60.6
Faulty	1.24	0.71	0.13	0.18	57.3

damage. As is evident from the vibration level, the bearing is more severely damaged in the first experiment when compared to the experiment in which both the motor and the pump bearing are damaged. However, the efficiency drop in both cases studied is comparable.

H. Application of the Proposed Fault Isolation Method to Other Pump Fault Types

The proposed model-based fault isolation method is tested for the three failure modes considered in this study. In this section, the proposed FIIC for the impeller fault case and the cavitation failure mode are shown. Again, since the proposed FII is insensitive to any failure in the pump, the fault cannot be detected using the propsoed FII. Since the input power required decreases because of the fault in the pump, the proposed FII decreases with the motor current RMS. Figure 59 shows the current RMS change and the proposed FIIC for two of the impeller fault cases with respect to the baseline "healthy" case. Figure 60 shows the current RMS change and the proposed FIIC for one of the cavitation fault levels.

Note that, for all the fault cases shown in the two figures, the current RMS drops as the input power decreases due to the fault in the pump (pump produces reduced work horsepower) and the proposed FII being insensitive to the pump faults also

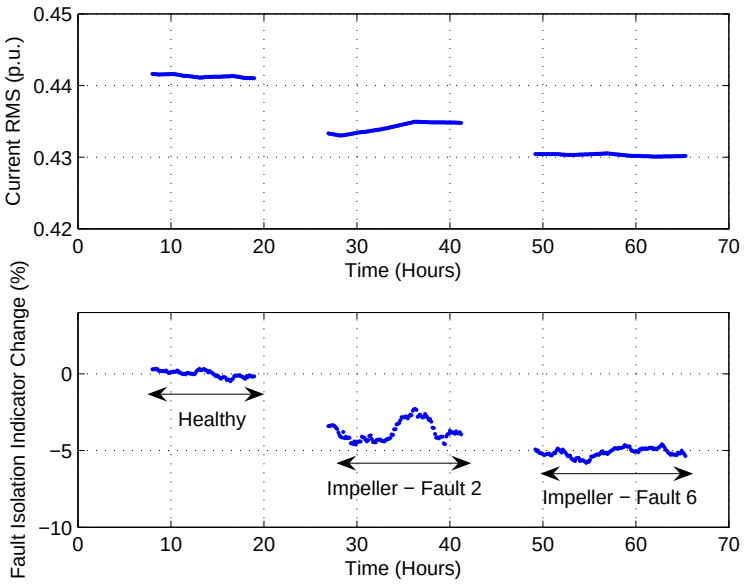

Fig. 59. Pump impeller fault; Current RMS change (top) ; Proposed FIIC (bottom).

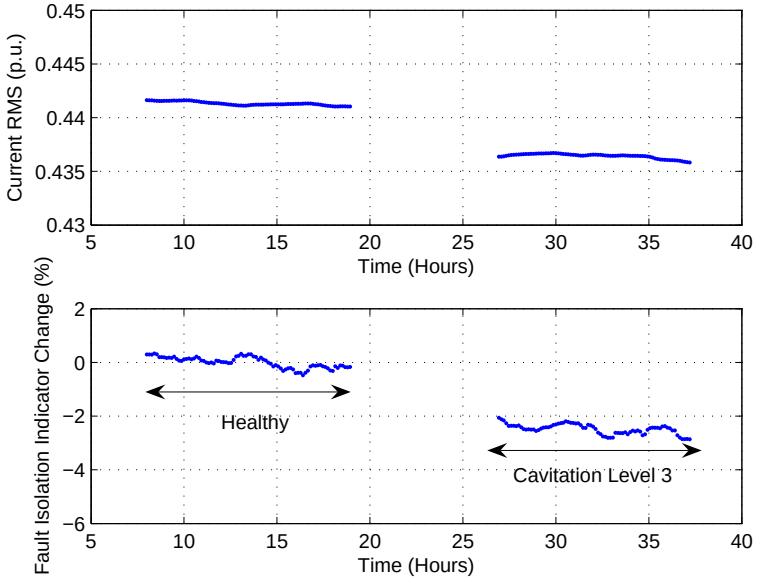

Fig. 60. Pump cavitation fault; Current RMS change (top); Proposed FIIC (bottom).

decreases.

I. Industrial Case Study

The proposed fault detection and isolation method uses only the measured motor electrical signals to detect faults in centrifugal pumps and to distinguish between motor and pump faults. No specific motor and/or pump model or design parameters are used in the development of these methods. Hence it can be easily ported to other similar motor-centrifugal pump systems of different power rating and manufacturer. Data from a motor-pump system installed at the Texas A&M University campus power plant is collected to ensure the portability of the proposed approaches. The motor is a $3-\phi$, 400 hp induction motor energized by constant frequency voltage from the power mains and drives a boiler feedwater pump. CT's and PT's are used to sample the motor currents and voltages, respectively.

Figure 61 shows the proposed FDIC for the sample data set. A load increase is detected on January 31, 2007 and hence the proposed method accounts for this load change and re-initializes the proposed FDIC. The proposed detects the presence of a fault within the system on February 1, 2007. The motor was shutdown for repairs on February 20, 2007. Hence the proposed method issues an alarm 19 days in advance. As mentioned earlier, the proposed FDIC alone is not sufficient to isolate the fault. Hence the proposed FII is computed. Figure 62 shows the current RMS change and the proposed FIIC for the data from February 15, 2007 to February 16, 2007. Referring to Table VII, it can be concluded that since the proposed FIIC increases, the fault is in the motor and not in the pump.

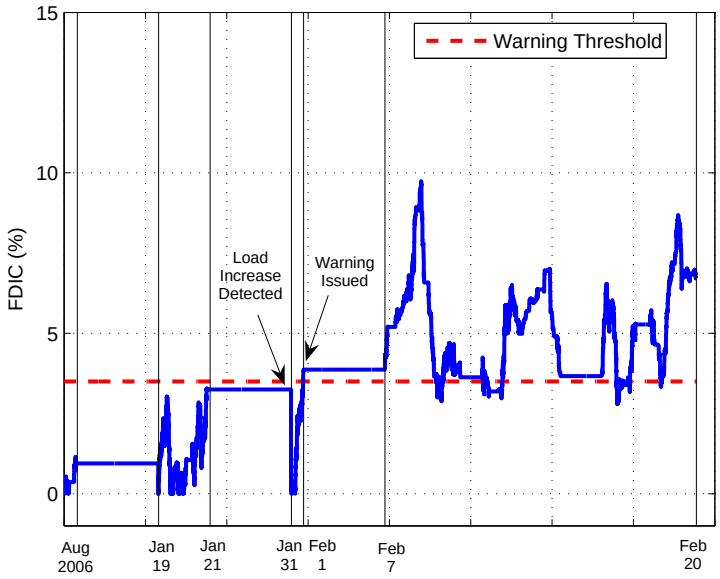

Fig. 61. Proposed FDIC for the sample data set from Texas A&M University campus power plant.

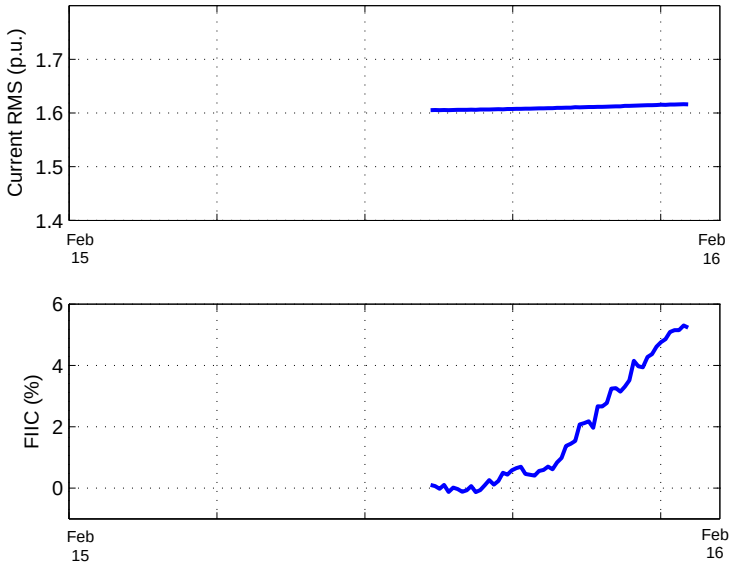

Fig. 62. Proposed FIIC for the sample data set from Texas A&M University campus power plant.

CHAPTER VI

SUMMARY AND CONCLUSIONS

A new approach for sensorless fault detection and isolation of centrifugal pumps is proposed.

A. Summary of Research

The objective of this research is to develop a model-based sensorless fault detection and isolation method for centrifugal pump problems. The developed model uses only the measured motor electrical signals and does not make use of motor and/or pump model and design parameters. Three pump failure modes are explored.

In Chapter I of the dissertation, a brief introduction on the state-of-the-art techniques used in the detection of centrifugal pump faults is discussed. The research objectives and a roadmap of the proposed method are also outlined. Finally, the contributions of this work are listed.

Chapter II describes an overview and the working principle of a centrifugal pump. The common failure modes of this type of pumps are also discussed in detail.

In Chapter III, an overview of fault detection methods is discussed. Differences between signal-based fault detection and model-based fault detection methods are outlined. Finally, the motivation for using a model-based fault detection scheme for centrifugal pump faults is described.

In Chapter IV, the proposed model-based fault detection method is explained in some detail. The development of the predictive model is described followed by the description of the fault indicator used in the detection of pump faults. This is followed by a detailed discussion of the proposed model-based fault isolation method. Finally, a description of the fault isolation indicator is provided.

In Chapter V, the experimental setup used to validate the performance of the proposed method is described. The staged fault detection results and the fault isolation results are also presented in detail. Vibration-based signal analysis is used as a reference for all of the experimental results.

B. Conclusions

The results of this study allow us to offer the following conclusions:

- The developed model-based fault detection method is capable of detecting incipient centrifugal pump faults with 100% detection capability and 0% false alarms.
- For the cracked impeller and the bearing damage case studies, the proposed detection method detects the presence of the fault before the vibration indicator detects the fault. However, for the cavitation case studies, the proposed method lags the vibration-based monitoring system, but it detects pump cavitation well in advance before any catastrophic failure.
- The developed model-based fault isolation method successfully distinguishes between motor faults and pump faults.
- The proposed approach uses only motor electrical signals. No motor and/or pump design parameters are used in the development of the fault detection and isolation method. Hence it can be easily ported to other similar motor-pump systems.

C. Recommendations for Future Work

This work shows that the developed sensorless fault detection and isolation method is capable of detecting faults in centrifugal pumps and also distinguish between motor faults and pump faults. Some of the topics for future research include:

- Identification of the specific type of centrifugal pump fault.
- Prediction of remaining useful life before failure.
- Detection and identification of other types of centrifugal pump faults, such as seal failures.

REFERENCES

[1] J. E. McInroy and S. F. Legowski, "Using power measurements to diagnose degradations in motor drivepower systems: A case study of oilfield pump jacks," in *IEEE Transactions on Industry Applications*, vol. 37, no. 6, pp. 1574-1581, November/December 2001.

[2] L. Bachus and A. Custodio, *Know and Understand Centrifugal Pumps*. New York: Elsevier Advanced Technology, 2003.

[3] C. J. Dister, "On-line health assessment of integrated pumps," in *Aerospace Conference Proceedings*, vol. 7, pp. 3289-3294, Big Sky, Montana, March 2003.

[4] J. A. Siegler, "Motor current signal analysis for diagnosis of fault conditions in shipboard equipment," *U.S.N.A – Trident Scholar Project Report*, no. 220, U.S. Naval Academy, Annapolis, Maryland, 1994.

[5] D. A. Casada, "Detection of pump degradation," in *22nd Water Reactor Safety Information Meeting*, Bethesda, Maryland, Oct, 1994.

[6] D. A. Casada and S. L. Bunch, "The use of the motor as a transducer to monitor pump conditions," in *P/PM Technology Conference*, Indianapolis, Indiana, December 1995.

[7] D. A. Casada, "Monitoring pump and compressor performance using motor data," in *ASME International Pipeline Conference*, vol. 2, pp. 885-895, 1996.

[8] D. A. Casada and S. L. Bunch, "The use of the motor as a transducer to monitor system conditions," in *Proceedings of the 50th meeting of the Society for Machinery Failure Prevention Technology*, pp. 661-672, Jan 1996.

[9] T. Kenull, G. Kosyna and P. U. Thamsen, "Diagnostics of submersible motor pumps by non-stationary signals in motor current," in *ASME Fluids Engineering Division Summer Meeting*, vol. 11, June 22-26, 1997.

[10] T. Dalton and R. Patton, "Model-based fault diagnosis of a two-pump system," in *Transactions of the Institute of Measurement and Control*, vol. 20, no. 3, pp. 115-124, 1998.

[11] S. Perovic, P. J. Unsworth and E. H. Higham, "Fuzzy logic system to detect pump faults from motor current spectra," in *Proceedings of 2001 IEEE Industry Applications Society 36th Annual Meeting - IAS'01*, vol. 1, pp. 274-280, September/October 2001.

[12] D. E. Welch, H. D. Haynes, D. F. Cox and R. J. Moses, "Electric fuel pump condition monitor system using electrical signature analysis," US Patent No: US 6,941,785, September 2005.

[13] H. D. Haynes, D. F. Cox and D. E. Welch,, "Electrical signature analysis (ESA) as a diagnostic maintenance technique for detecting the high consequence fuel pump failure modes," *Presented at Oak Ridge National Laboratory*, October, 2002.

[14] C. S. Kallesoe, V. Cocquemptot and R. Izadi-Zamanabadi, "Model based fault detection in dentrifugal pump application," in *IEEE Transactions on Control Systems Technology*, vol. 14, no. 2, pp. 204-215, March 2006.

[15] E. P. Sabini, J. A. Lorenc and O. Henyan, "Centrifugal pump performance degradation detection," US Patent No: US 6,648,606 B2, November 2003.

[16] S. C. Schmalz and R. P. Schuchmann, "Method and apparatus of detecting low

flow/cavitation in a centrifugal pump," US Patent No: US 6,709,240 B1, March 2004.

[17] C. A. Harris, J. A. Schibonski, F. E. Templeton and D. L. Wheeler, "Pump system diagnosis," US Patent No: US 6,721,683 B2, April 2004.

[18] K. Kim, A. G. Parlos and R. M. Bharadwaj "Sensorless fault diagnosis of induction motors," *IEEE Transactions on Industrial Electronics*, vol. 50, no. 5, pp. 1038-1051, 2003.

[19] K. Kim and A. G. Parlos, "Reducing the impact of false alarms in induction motor fault diagnosis," *Journal of Dynamic Systems, Measurement and Control*, vol. 125, no. 1, pp. 80-95, 2003.

[20] Virginia Technology, "Pumps," http://www.cee.vt.edu/program_areas/environmental/teach/wtprimer/pumps/ pumps.html. Accessed on February 11, 2004.

[21] F. R. Spellman and J. Drinan, *Fundamentals for the Water and Wastewater Maintenance Operator Series: Pumping*. Pennsylvania: Technomic Publishing Company, 2001.

[22] Energy Manager Training, "Industrial pumps," http://www.energymanagertraining.com/eqp_ind_pumps.htm. Accessed on January 21, 2004.

[23] S. Yedidiah, *Centrifugal Pump User's Guidebook: Problems and Solutions*. New York: International Thomson Publishing Company, 1996.

[24] Hargrave Corporation, "Common pump problems," http://www.hargrave.com.my/about_pumps.php?page= 5. Accessed on December 12, 2006.

[25] Depco Pump Company, "Troubleshooting guide," http://www.depcopump.com/catalog107/149.pdf. Accessed on January 28, 2004.

[26] World Pumps, "Pump maintenance," http://www.worldpumps.com/WZ/World Pumps/latestfeatures/maintenance/ 000021/show. Accessed on January 28, 2004.

[27] G. mendles and B. Larose, "Pump and seal failure analysis improves reliability, reduces costs," in *Enery-Tech Magazine*, January 2007.

[28] U.S. Department of Energy, "Reactive maintenance," http://www.eere.energy.gov/femp/operations_maintenance/strategies/strat_reactive.cfm. Accessed on December 13, 2006.

[29] R. J. Patton and J. Chen, "Robustness in quantitative model-based fault diagnosis," in *IEE Colloquium on Intelligent Fault Diagnosis - Part 2: Model-Based Techniques*, pp. 4/1-4/17, 1992.

[30] P. P. Harihara, K. Kim and A. G. Parlos, "Signal-based versus model-based fault diagnosis - a tradeoff in complexity and performance," in *IEEE International Symposium on Diagnostics for Electric Machines, Power Electronics and Drives (SDEMPED 2003)*, pp. 277-282, Atlanta, Georgia, August 24-26, 2003.

[31] R. C. Dugan, M. F. McGranaghan, S. Santoso and H. W. Beaty, *Electrical Power Systems Quality*. New York: McGraw-Hill, 2003.

[32] P. C. Krause, O. Wasynczuk and S. D. Sudhoff, *Analysis of Electric Machinery*. New York: The Institute of Electrical and Electronics Engineers, Inc., 1995.

[33] C. L. Nikias and A. P. Petropulu, *Higher-Order Spectra Analysis - A Nonlinear Signal Processing Framework*. New Jersey: PTR Prentice Hall, 1993.

[34] J. R. Stack, R. G. Harley and T. G. Habetler, "An amplitude modulation detector for fault diagnosis in rolling element bearings," in *IEEE Transactions on*

Industrial Electronics, vol. 51, no. 5, pp. 1097-1102, October 2004.

[35] L. Wang, "Induction motor bearing fault detection using a sensorless approach," Ph.D Dissertation, Mechanical Engineering, Texas A&M University, College Station, May 2007.

[36] J.R. Stack, "Experimentally generating faults in rolling element bearings via shaft current," *IEEE Transactions on Industry Applications*, vol. 41, No. 1, January/February 2005.

[37] H. Prashad, "Diagnosis of rolling-element bearings failure by localized electrical current between track surfaces of races and rolling-elements," *Journal of Tribology*, vol. 124, no. 3, pp. 468- 473, July 2002.

[38] D.F. Busse, J.M. Erdman, R.J. Kerkman, D.W. Schlegel, and G.L. Skibinski, "The Effects of PWM voltage source inverters on the mechanical performance of roller bearings," *IEEE Transactions on Industry Applications*, vol. 33, No. 2, pp. 567-576, March/April 1997.

[39] *IEEE Standard Test Procedure For Polyphase Induction Motors and Generators*. New York: IEEE Power Engineering Society, November 2004.

APPENDIX A

MOTOR MECHANICAL OUTPUT POWER AND ELECTRICAL INPUT POWER CALCULATIONS

Table X and Table XI outlines the steps required to calculate the motor output power and the electrical input power based on the IEEE 112 standard. The parameter k_1 used in the calculations is a constant equal to 234.5 for 100% IACS conductivity copper or 225 for aluminium, based on a volume conductivity of 62%. The last column in the tables describe how the test points are obtained. The different test points, described in the second column, can be obtained either by measuring the value using a multimeter or by using a pre-determined formulae.

Table X. Motor mechanical output power calculations.

Steps	Test Point	Source or Calculation
1	Specified temperature, t_s, in ^{o}C	From IEEE 112 chart
2	Line-to-Line voltage, in V	Measurement
3	Frequency, in Hz	Compute from FFT of voltage signal
4	Synchronous speed, n_s, in r/min	$\frac{120 \times \text{Frequency}}{\text{Number of poles}}$
5	Stator resistance, in Ohms	Measurement
6	Ambient temperature, in ^{o}C	Measurement
7	Stator winding temperature, t_t in ^{o}C	Measurement
8	Observed speed, in r/min	Measurement
9	Observed slip, in r/min	(4) − (8)
10	Observed slip, in p.u.	(9)/(4)
11	Corrected slip, in p.u.	$(10) \times \frac{[k_1+(1)]}{[k_1+(7)]}$
12	Corrected speed, in r/min	$(4) \times [1 - (11)]$
13	Torque, in N/m	Measurement
14	Shaft power, in W	$(13) \times (12)/9.549$

Table XI. Motor electrical input power calculations.

Steps	Test Point	Source or Calculation
1	Specified temperature, t_s, in ^{o}C	From IEEE 112 chart
2	Line-to-Line voltage, in V	Measurement
3	Frequency, in Hz	Compute from FFT of voltage signal
4	Synchronous speed, n_s, in r/min	$\frac{120 \times \text{Frequency}}{\text{Number of poles}}$
5	Stator resistance, in Ohms	Measurement
6	Ambient temperature, in ^{o}C	Measurement
7	Stator winding temperature, t_t in ^{o}C	Measurement
8	Line current, in A	Measurement
9	Stator power, in W	$\int v(t)i(t)dt$
10	Stator I^2R loss, in W at t_t	$1.5 \times (8)^2 \times (5) \times \frac{[k_1+(7)]}{[k_1+(6)]}$
11	Winding resistance at t_s	$(5) \times \frac{[k_1+(1)]}{[k_1+(6)]}$
12	Stator I^2R loss, in W at t_s	$1.5 \times (8)^2 \times (5) \times (11)$
13	Stator power correction	$(12) - (10)$
14	Electrical input power, in W	$(9) + (13)$

VITA

Parasuram Padmanabhan Harihara was born in Palakkad, Kerala, India. He received his B.E degree in Mechanical Engineering from Osmania University, Hyderabad, in 1999. He received his M.S degree also in Mechanical Engineering from Texas A&M University, College Station, in 2002. His research interests include condition monitoring and fault diagnosis of mechanical and electro-mechanical systems, system identification and control systems design.

Parasuram P. Harihara may be reached at Flat 301, Gharonda Lanka, Street 5, Jawahar Nagar, Hyderabad, 500020, India. His email address is pharihara@yahoo.com

The typist for this dissertation was Parasuram P. Harihara.